The Journal of Membrane Biology (2021) 254:217–237
https://doi.org/10.1007/s00232-021-00177-y

A Protein and Membrane Integrity Study of TiO_2 Nanoparticles-Induced Mitochondrial Dysfunction and Prevention by Iron Incorporation

Tejal Barkhade[1] · Santosh Kumar Mahapatra[2] · Indrani Banerjee[1]

Received: 26 November 2020 / Accepted: 19 March 2021 / Published online: 31 March 2021

Abstract

The paper assessed the toxic effect of titanium dioxide (TiO_2) nanoparticles (NPs) on isolated mitochondria and its dysfunction prevention after Iron (Fe) incorporation. TiO_2 and Fe content TiO_2 NPs were synthesized and characterized using XPS, PL spectroscopy, and TEM. The nanostructure interaction with isolated mitochondria was investigated using circular dichroism (CD) confocal microscopy, flow cytometry, atomic force microscopy (AFM), surface-enhanced Raman spectroscopy (SERS), and FT-IR spectroscopy via nonspecific pathway. Fe content TiO_2 NPs helps to control the dissolution rate of parent nanomaterial of TiO_2 on the mitochondrial membrane. Confocal micrographs and flow cytometry results confirmed that Rhodamine 123 dye intensity get increased after interaction with Fe content TiO_2 NPs which states the integrity of the mitochondrial membrane. AFM results revealed that TiO_2 induces the swelling of mitochondrial tubules and also impaired the mitochondrial structure, whereas Fe content TiO_2 NPs interaction prevents the impairment of mitochondrial tubules. The denaturation of a membrane protein by TiO_2 interactions was observed through CD Spectroscopy. Further, nano-bio-interface study was performed using SERS, through shifting and extinct of peaks affiliated to membrane proteins and lipids. However, Fe content TiO_2-treated samples showed a significant increase in the membrane potential of mitochondria via flow cytometry results.

Graphic Abstract

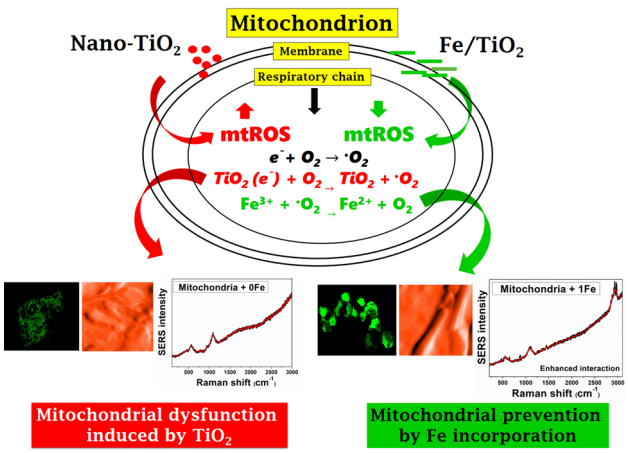

Keywords Mitochondria · Fe content TiO_2 · Protein · Toxicity · Nanoparticles · Interaction · Membrane

✉ Indrani Banerjee
indrani.banerjee@cug.ac.in

Extended author information available on the last page of the article

Introduction

Nanotoxicology has emerged only recently, years after the first thriving of nanotechnology when numerous nanomaterials had already been introduced into a number of industrial processes and products (Elsaesser and Howard 2012). More concerns on health risks about exposure to nanoparticles have been rising. Nanomaterials in the range of 0.1–100 nm could easily enter into the human body. It has unique physicochemical, optical, and electrical properties (Jefferson 2000; Takenaka et al. 2001; Kreyling et al. 2002). Nano-TiO_2 is broadly applied in cosmetics, food, personal care products, and biomedical applications, and so on because of its unusual features (Jacobs et al. 2010; Weir et al. 2012). However, when the size of TiO_2 is reduced to the nanoscale, the bio-activity and physiochemical properties of nano-sized TiO_2 are significantly different from the properties of their bulk size (Donaldson et al. 2000; Oberdörster et al. 2005).

TiO_2 has been used for several years as an inert, nontoxic pigment product or other substance assessed by many regulatory bodies such as the Material Safety Data Sheets (MSDS). The US Food and Drug Administration (FDA) permitted for its ingestion as drug additive, external use including the eye area, and considered it as a safe substance for public health (Hwang et al. 2019; Banerjee and Thiagarajan 2014). However, several studies have confronted the permitted use of nano-TiO_2 (Bennat and Muller-Goymann 2000; Mavon et al. 2007; Warheit et al. 2007; Wang et al. 2007). Since nanoparticles diameter does not exceed a hundred nanometres at maximum, they are able to penetrate cells and interfere with several sub-cellular mechanisms or organelles. Nano-TiO_2 has been studied mainly with recognized in vitro toxicity assays that analyse major cellular parameters such as cytotoxicity, enzyme activities, genotoxicity, and response to many stress factors (Santonastaso et al. 2019; Chibber and Agarwal 2017; Jin et al.2008; Natarajan et al. 2015). In vivo toxicity measures of nano-TiO_2 on different main organs are also reported (Trouiller et al. 2009; Chen et al. 2009; Wu et al. 2009). Indeed, some studies showed that nano-TiO_2 can penetrate in mitochondria which is a principal organelle of the body cells and hence may directly interfere with the structure and its function (Barkhade et al. 2019a; Freyre-Fonseca et al. 2011; Chen et al. 2018). Mitochondria play an extremely important role in regulating cell functioning including adenosine triphosphate (ATP) synthesis to generate energy. It was reported that TiO_2 has the potential to demolish adenine and phosphate moieties of energy biomolecule ATP (Barkhade et al. 2019b).

There are many approaches to reduce the toxicity of nanomaterials like surface coating, functionalization, and metal incorporation (Pelaz et al. 2015; Osmond-McLeod et al. 2014; Saleh et al. 2016). We preferred the incorporation of Fe ions into TiO_2 lattice because Fe^{3+} having a radius of 0.64 Å similar to Ti^{4+} 0.68 Å can be easily incorporated inside the TiO_2 matrix (Nasralla et al. 2013). The purpose of the Fe incorporation was to reduce the toxic effect of TiO_2 and its rate of dissolution at the sub-cellular level (George et al. 2011; Flak et al. 2015). However, the approach of Fe addition has been reported previously to decrease the toxicity of ZnO nanomaterial (Xia et al. 2011; Li et al.2011). Toxicological effects of nano-TiO_2 on HBL-100 cells were studied earlier by our group (Barkhade et al. 2019c).

In the present study, we are trying to investigate the interaction of TiO_2 and Fe content TiO_2 nanoparticles with isolated mitochondria using flow cytometry, confocal imaging, atomic force microscopy, surface-enhanced Raman scattering facilities and infrared spectroscopy which demonstrated the mitochondrial dysfunction due to TiO_2 interaction and prevented by Fe content TiO_2 nanoparticles.

Experimental

Chemicals

Ethanol (C_2H_6O, ~ 96%), tetraisopropyl (IV) isopropoxide (TTIP, $Ti[OCH(CH_3)_2]_4$, 99.99%), anhydrous iron (III) chloride ($FeCl_3$, ≥ 99.99%), ethylenediaminetetra acetic acid (EDTA, ≥ 98.5%), ethylene glycol-bis(2-aminoethylether)-*N,N,N′,N′*-tetraacetic acid (EGTA, ≥ 97.0%), rhodamine 123 (mitochondrial-specific fluorescent dye), 2′,7′-Dichlorofluorescin diacetate (DCFH-DA, ≥ 97%), mannitol ($C_6H_{14}O_6$, ≥ 96%), sucrose ($C_{12}H_{22}O_{11}$, ≥ 99.5%), bovine serum albumin (BSA, ≥ 98%), tri-hydrochloride ($NH_2C(CH_2OH)_3$.HCl), 4-(2-Hydroxyethyl) piperazine-1-ethane sulfonic acid (HEPES, $C_8H_{18}N_2O_4S$, ≥ 99.5%), and hydrochloric acid (HCl, 36.5–38.0%, BioReagent) chemicals were procured from Sigma Aldrich, India. Dounce tissue grinder set (7ML complete) was also purchased from Sigma Aldrich. Deionized water was used throughout the reactions. Fresh chicken liver tissue was acquired from the near slaughterhouse. All other reagents were of analytical reagent grade, and all solutions were prepared with deionized (DI) water. All glasswares were washed with dilute nitric acid (HNO_3) and distilled water and dried in hot air oven before performing the experiments.

Buffers Preparation

Buffer A contains 0.22 mol/L mannitol, 0.07 mol/L sucrose, 0.02 mol/L HEPES, 2 mmol/L Tris–HCl, and 1 mmol/LEDTA, and 0.4% BSA. Buffer B contains 0.22 mol/L

mannitol, 0.07 mol/L sucrose, 0.01 mol/L Tris–HCl, and 1 mmol/LEDTA. Buffer C contains 0.22 mol/L mannitol, 0.07 mol/L sucrose, and 1 mmol/L EDTA. The pH of buffers was kept 7.4.

Preparation of TiO_2 and Fe Content TiO_2 Nanoparticles

The pure TiO_2 and Fe content TiO_2 powder samples with different concentration of Fe^{3+} were prepared through the conventional sol–gel method (Barkhade et al. 2019b; Mathews et al. 2015). In the synthesis process, 4 mL of TTIP was dissolved in 20 mL of ethanol, on continuous stirring for 1 h, in which 1 mL of HCl was added to get a clear transparent solution. Different molar (M) concentration of $FeCl_3$ solution, i.e. 0, 0.1, 0.5, and 1 was added batch-wise to clear transparent solution of TTIP and kept on a stirrer for 2 h at room temperature and samples named as 0Fe, 0.1Fe, 0.5Fe, and 1Fe, respectively. The pH about 2.0 was maintained during all the steps of the synthesis process. Finally, distilled water was slowly added to the solution by stirring for 1 h. The solution was dried at 80 °C and calcined at 500 °C for 3 h. The synthesized powder was finally grounded and submitted for characterization.

Characterizations of TiO_2 and Fe Content TiO_2 Nanoparticles

The structural and the chemical state of synthesized nanostructured materials were analysed employing high-resolution X-ray photoelectron spectroscopy (XPS) spectra (PHI 5000 Versa Probe III). The photoluminescence (PL) spectroscopy was done to study the lattice defects in the samples and PL spectra were recorded at ambient temperatures using Fluorolog, Horiba FL-1057 instrument. Morphology, shape, size, and surface characteristics of the nanoparticles were determined with transmission electron microscopy (TEM, Jeol/JEM 2100) at 200 kV accelerating voltage. For TEM, the samples were dispersed in ethanol, sonicated and deposited onto carbon-coated copper grids. Particle diameter was determined using Image J software to count the particles seen in TEM images acquired from a different area in each sample.

Nanoparticle Size Distribution Calculation Using Image J

Image J is a Java-based image processing program established at the National Institutes of Health (NIH) for the analysis of particles size distribution from the selected TEM image. After selection of specify area in TEM image, analyse and set measurements command were used to analyse the particle size. This command counts and measures objects in threshold images. Then after scanning the image or selection until it finds the edge of an object. It then outlines the object using the wand tool, and measures it using the measure command. The dialog box was used to configure the particle analyser. Then, the summary of the particle count and area is shown in another data window and data were saved in excel sheet. Further, calculation was done using the below formulas (1), (2), and (3) for size distribution.

$$\text{Area} = \pi r^2 \tag{1}$$

$$r = \sqrt{A/\pi} \tag{2}$$

$$\text{Diameter (D)} = 2 \times r \tag{3}$$

Isolation of Mitochondria

Mitochondria were isolated from chicken liver tissue using standard differential centrifugation process. The fresh liver tissue was crushed on an ice bath and then homogenized with Dounce Tissue Grinder in buffer A. The homogenate was centrifuged at 3000×*g* for 3 min. Then the supernatant was centrifuged at 17,500×*g* for 5 min. The resulting pellets were washed with buffer A and centrifuged at 17,500×*g* for 5 min. Then, the pellets were resuspended in buffer B and centrifuged at 17,500×*g* for 5 min. The pellets were lastly resuspended in buffer C and kept at 4 °C. The mitochondrial protein concentration was determined by the Biuret method taking BSA protein as the standard (Yang et al. 2016).

Reactive Oxygen Species (ROS) Generation Test

Dosage of 50 and 100 µg/mL of 0Fe, 0.1Fe, 0.5Fe, and 1Fe incubated with isolated mitochondrial pellet (1 mg/mL) in buffer C at 37 °C for 30 min. Then the DCFH-DA probe was mixed with the mitochondrial-nanoparticle suspension for 30 min and kept under room temperature. The increasing rate of fluorescence of DCFH-DA (ex: 488 nm; em: 525 nm, 250 nM) indicated the ROS generation of mitochondria. The fluorescence intensities were measured using an FP-6500 Jasco Spectrofluorometer.

Flow Cytometry

Mitochondrial membrane potential was determined by the changes of fluorescent intensity of Rh123, detected by C6 Accuri BD flow cytometer. Isolated mitochondrial fractions in buffer C (1 mg/mL) were incubated with various concentrations of TiO_2 and Fe content TiO_2 (0Fe, 0.1Fe, 0.5Fe, 1Fe) for 30 min. After that 2 µmol/L of Rhodamine 123 mitochondrial membrane probe was preloaded for 30 min in dark at 37 °C. The unbound dye was removed by centrifugation. After centrifugation, the pellets were resuspended in

buffer C and detected with a flow cytometer to collect the fluorescence of FL-1 channel (excitation: 488 nm; emission: 511 nm) (Freyre-Fonseca et al. 2011).

Confocal Imaging

Isolated mitochondrial fractions in buffer C (approx. 1 mg) were incubated with various concentrations of TiO_2 (0Fe) and Fe content TiO_2 (0.1Fe, 0.5Fe, 1Fe) for 30 min. After that, 2 µmol/L Rhodamine 123 was preloaded for 30 min in dark at 37 °C. The unbound dye was removed by centrifugation. After centrifugation, the wet pellets were spread on the surface of a glass slide and imaged using confocal microscopy (Olympus FV500 IX 81).

Atomic Force Microscopy (AFM)

Isolated mitochondria (1 mg/mL) were interacted with 0Fe, 0.1Fe, 0.5Fe, and 1Fe nanoparticles solutions and kept under 37 °C for one hour before analysis. The experiments were conducted using the Nanosurf C3000 atomic force microscopy (AFM). The 50 µL mitochondrial nanoparticles-interacted solution was placed on a freshly cleaved mica plate that is nearly smooth, incubated for 10 min, and then the residual solution was blown by a stream of nitrogen. The measurements were made at ambient temperature using a silicon nitride tip with tapping mode by varying resonance frequencies at a linear scanning rate of 0.5 Hz.

Surface-Enhanced Raman Scattering (SERS)

The isolated mitochondrial fraction was gently added in 20 µL of 0Fe, 0.1Fe, 0.5Fe, and 1Fe nanoparticles solution for utilization of mitochondria in SERS facility. Prepared mitochondria–nanoparticle suspensions were incubated for approximately 10 min at room temperature. Then, a 5 µL of the mixed suspension was dropped onto the glass slides and waited for several minutes until most of the water dried from the droplet. Prepared samples were analysed with a completely automated Renishaw Invia Raman Microscopy System equipped with an 830 nm diode and 514 nm argon-ion laser. The laser power was arranged for the range of 0.5–6 mW and the exposure time was 10 s for the 830 nm diode laser that was utilized in our measurements.

Circular Dichroism (CD) Spectroscopy

The alteration in membrane-associated protein structure after treatment with synthesized nanoparticles was investigated. Briefly, the mitochondrial protein (0.2 mg/mL) was added to each 0Fe, 0.1Fe, 0.5Fe, and 1Fe nanoparticle solutions and then incubated for 1 h at room temperature. The spectra were obtained over the wavelength range of 200–260 nm with quartz cuvette of 1.0 cm path length using Jasco J-815 CD spectrometer at ambient temperature (Kelly and Price 2000). The time constant of 10 s was used. The baseline was obtained with the buffer which contained 0.22 mol/L mannitol, 0.07 mol/L sucrose, and 1 mmol/L EDTA, pH 7.4.

Fourier-Transform Infrared Spectroscopy (FT-IR) Spectroscopy

FT-IR spectroscopy is an admirable tool for the investigation of mitochondrial membrane protein interactions. The synthesized TiO_2 and Fe content TiO_2 (0Fe, 0.1Fe, 0.5Fe, 1Fe) was suspended in a 1 mg/mL of isolated mitochondrial solution in buffer C (pH 7.4). The nanoparticles-loaded mitochondrial protein samples were kept for 1 h at ambient temperature. The FT-IR spectra were recorded in the range of 400–4000 cm^{-1} using SP-65 Perkin–Elmer spectrometer.

Statistical Analysis

The dataset from three to four independent experiments were submitted to statistical analysis and were expressed as mean ± standard deviations (SDs).

Results and Discussion

XPS Analysis

The change in the binding energy of TiO_2 and Fe content TiO_2 nanocomposites were investigated by XPS analysis. XPS being a surface-sensitive technique provides information about the change in the chemical state of the species constituting the material (Hirano et al. 2004). Figure 1 shows the XPS survey spectra of synthesized 0Fe, 0.1Fe, 0.5Fe, and 1Fe samples. In these spectra, C1s is an instrumental impurity. The peaks corresponding to Ti2p and O1s were observed in 0Fe sample, whereas the peak for Fe starts originating for the rest of the Fe content samples. The peak intensities of Ti2p and O1s reduce with an increase in Fe concentration in the sample. The peak intensities of Fe content TiO_2 samples decrease with an increase in addition of Fe concentration. Fe-incorporated titanium dioxide has Ti/O ratio different to pure one and decreasing with an increase in Fe concentration. This can be attributed to the presence of Fe on the surface of TiO_2.

High-resolution XPS core-level spectrum of Fe2p was measured in order to evaluate the electronic nature of Iron in Fe content TiO_2 (0.1Fe, 0.5Fe, 1Fe) nanoparticles calcined at 400 °C. Fe content in TiO_2 results in a minor shift in the binding energy, indicating that Fe ions are well dispersed in the substitutional sites of TiO_2 lattice and produce new

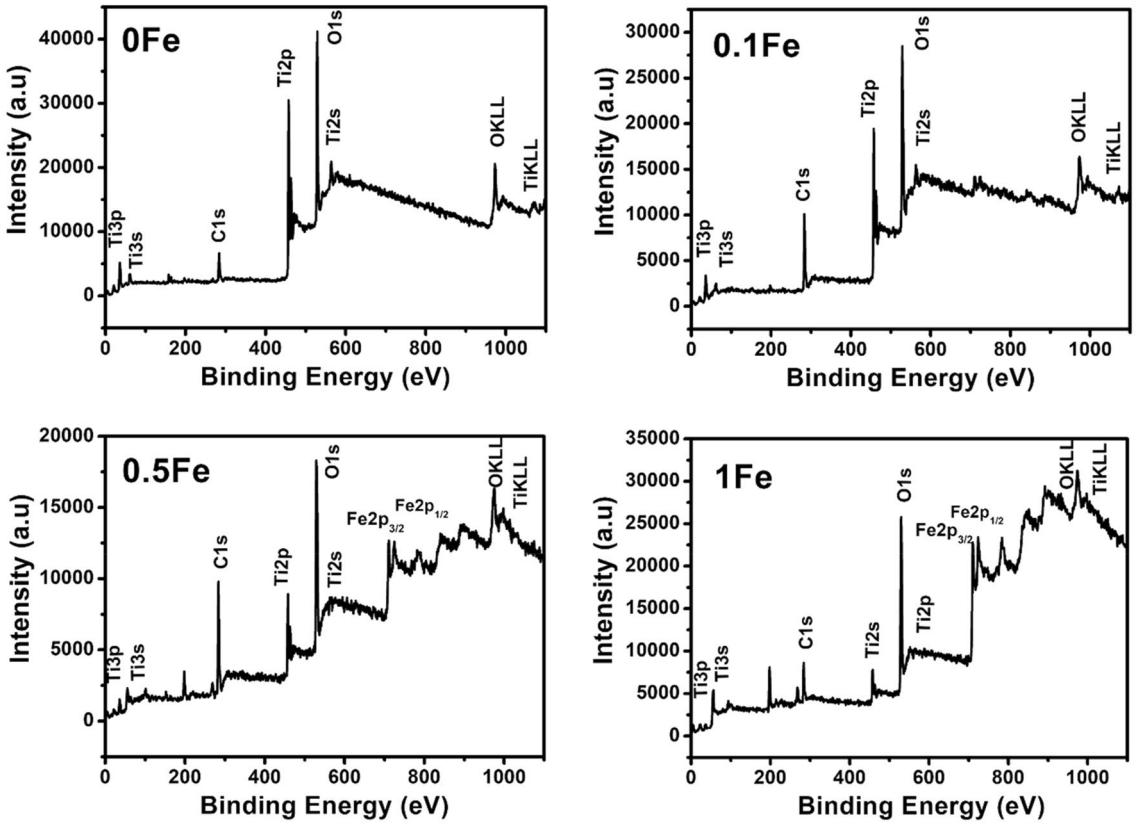

Fig. 1 XPS survey spectra of synthesized 0Fe, 0.1Fe, 0.5, and 1Fe nanoparticles

mixed oxide structure, possibly Fe–O–Ti. Figure 2a–c shows high-resolution spectrum of Fe2p. Binding energies of Fe^{3+} for $Fe2p_{3/2}$ were observed at 710.07 eV, 710.22 eV, and 710.39 eV for samples 0.1Fe, 0.5Fe, and 1Fe, respectively. A very weak peak at 711.71 eV is also observed, suggesting the presence of a minor portion of Fe^{2+} ions. By considering the initial sol–gel of Iron (III) chloride 6-anhydrous, it would also be expected that Fe would exist mainly in the + 3 oxidative state (Fe^{3+}) (Bharti et al. 2016). The binding energies of $Fe2p_{1/2}$ spectrum are observed at 723.43 eV to 723.84 eV and 723.91 eV for 0.1Fe, 0.5Fe, and 1Fe, respectively, with an increase in Fe content in the samples. The intensity of Fe2p increased with the increase in the concentration of Fe in the sample. The presence of satellite peak at 718.9 eV indicates that Fe is present in Fe^{3+} ionic state.

The high-resolution spectrum of O1s for TiO_2 and Fe content TiO_2 samples are shown in Fig. 3. O1s spectrum is assigned to binding energy 528.58 eV of lattice oxygen and binding energy 529.87 eV is assigned to oxygen in $Ti_2O_3$for 0Fe sample which is shown in Fig. 3a. A slight shift in the position of O1s and Ti_2O_3 along with variation in the intensity of peak was observed after Fe incorporation which is shown in Fig. 3b–d. After Fe incorporation, the peaks get shifted to binding energies at 528.54 eV, 528.77 eV, and 528.78 eV for 0.1Fe, 0.5Fe, and 1Fe, respectively, corresponding to O1s (Ti–O). Table 1 presents the consolidated peak positions and shifting for all the components present in the system. It can be seen that O1s peak intensity decreased due to the formation of Fe–O bonds on the surface of TiO_2. The peak intensity of Ti_2O_3 increased with an increase in Fe concentration. After Fe incorporation, the peaks get shifted to binding energies at 530.26 eV, 530.53 eV, and 530.16 eV for to 0.1Fe, 0.5Fe, and 1Fe, respectively, corresponding to Ti_2O_3.

Figure 4 shows the high-resolution XPS spectrum of Ti2p of pure TiO_2 and Fe content TiO_2 samples. The spectrum contains two main peaks of $Ti2p_{3/2}$ (binding energy 457.36 eV) and $Ti2p_{1/2}$ (binding energy 463.15 eV) arising from spin orbit-splitting for pure TiO_2 (0Fe) sample as shown in Fig. 4a. These peaks are consistent with Ti^{4+} in TiO_2 lattice. Ti2p spectrum typically appears in Ti^{4+} oxidation state with a small influence of Ti^{3+}. This indicates the formation of Ti^{3+}occurring due to O_2 deficiency in the lattice. After incorporation of Fe at different concentration, the high-resolution XPS spectrum in Fig. 4b–d shows a slight shift in the position along with a variation in the area under the peaks. The peak position of $Ti^{4+}2p_{3/2}$ in the Fe content TiO_2 samples is observed slightly at higher binding

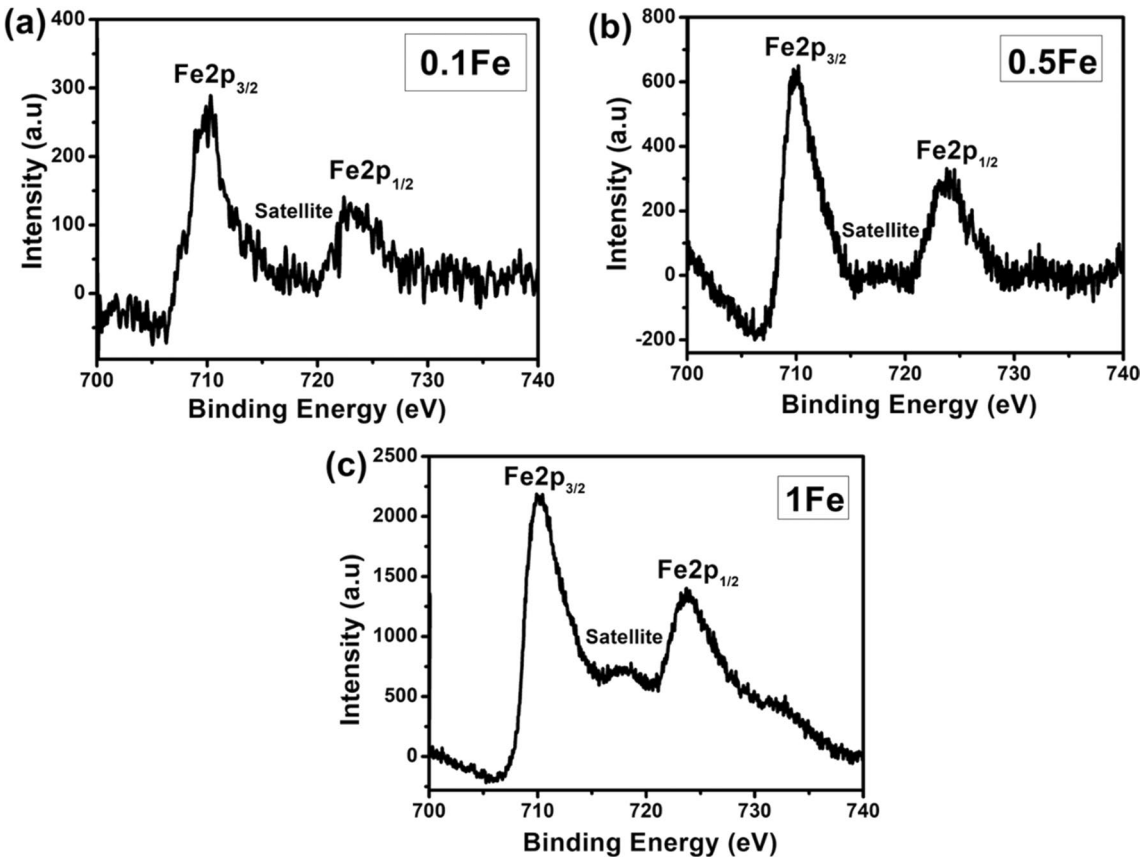

Fig. 2 High-resolution spectra of Fe2p of **a** 0.1Fe, **b** 0.5Fe, and **c** 1Fe nanoparticles

energies of 457.38 eV, 457.58 eV, and 457.59 eV for 0.1Fe, 0.5Fe, and 1Fe, respectively. The peak position of $Ti^{4+}2p_{1/2}$ in the Fe content TiO_2 samples is situated at higher binding energies of 463.43 eV, 463.50 eV, and 463.51 eV for 0.1Fe, 0.5Fe, and 1Fe, respectively. Typically, the FWHM of each spin–orbit component of Ti2p seems to be same. However, the Ti2p component is broader than that of $Ti2p_{3/2}$for all samples. Consequently, $Ti2p_{1/2}$ is much shorter than $Ti2p_{3/2}$ due to Coster–Kronig effect (Bapna et al. 2011).

The splitting values for Ti2p components increase from 5.79 eV, 6.05 eV, 5.92 eV, and 5.92 eV for increase in Fe concentration in TiO_2. The shift in the position of these peaks indicates an influence of Fe addition on the electronic state of Ti element, probably some of the Ti ions get substituted with Fe ions in the lattices because of the almost same ionic radius. $Ti^{4+}2p_{3/2}$ peaks are observed to be shifted to 0.23 eV in 1Fe sample from virgin state sample indicating the formation of Fe–O–Ti bonds which is in agreement with earlier reports (Abidov et al. 2013; Leedahl et al. 2014). The very highly intense peak of pure TiO_2 shows declines in intensity with the increase of Fe concentration in the TiO_2 matrix. Meanwhile, decreasing area of Ti^{4+} indicates a reduction of TiO_2 in the sample and probably the formation of Ti–O–Fe structure in theTiO_2 lattice through substitution of transition metal ions. Table 2 shows the ratio of area under the curve for oxygen/Ti ratio. The observed shift in the peaks also indicates interaction between Ti and Fe atoms and overlapping of their 3d orbital (Wang et al. 2009). This causes an electronic excitation from Fe to Ti in the optical absorption experiment, which shows a reduction in the band gap of Fe content TiO_2 nanocomposites as observed in the optical analysis.

Photoluminescence Spectroscopy

Figure 5a–d shows the photoluminescence spectra of the 0Fe, 0.1Fe, 0.5Fe, and 1Fe samples excited at 325 nm, respectively, at room temperature. The peak in the UV region around 339 nm is attributed to the near-band-edge excitonic emission (NBE), as the energy corresponding to this peak is close to the bandgap energy (3.49 eV) of TiO_2 (Ali et al. 2017). The peak broadening was noticed possibly because of the presence of several recombination sites and defects in Fe content TiO_2 samples, which could be attributed to the self-trapped excitons and defects associated with oxygen vacancy states in TiO_2 (Akshay et al.

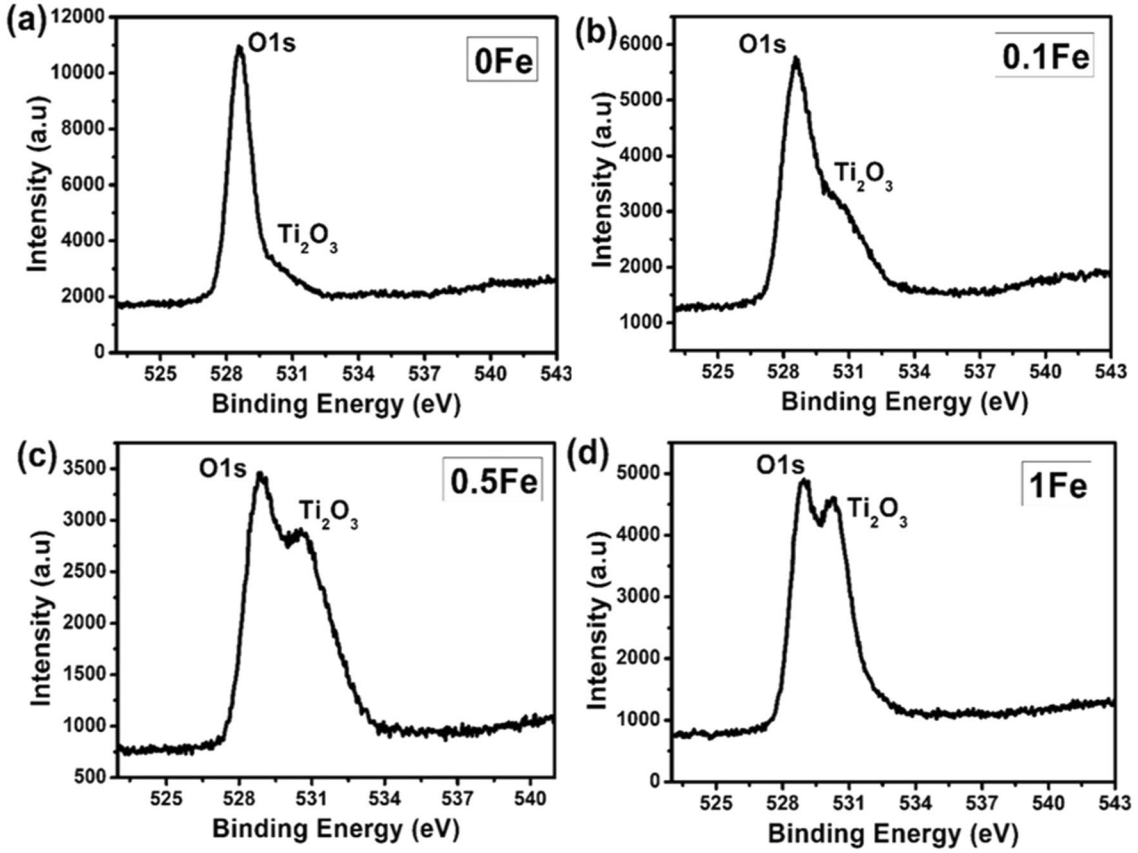

Fig. 3 High-resolution spectra of O1s **a** 0Fe, **b** 0.1Fe, **c** 0.5Fe, **d** 1Fe nanoparticles

Table 1 Peak shifts in Ti2p and O1s XPS spectrum after Fe incorporation into TiO_2

Samples	Peak Positions (eV)			
0Fe	$Ti^{4+}2p_{3/2}$ 457.36	$Ti^{4+}2p_{1/2}$ 463.15	O1s 528.58	Ti_2O_3 529.87
Peak Shift after Fe incorporation				
0.1Fe	457.38	463.43	528.54	530.26
0.5Fe	457.58	463.50	528.77	530.53
1Fe	457.59	463.51	528.78	530.16

2019). The UV emission band can be explained by near-band-edge transition originating from the recombination of carriers bound within excitons. The peak at around 416 nm originates from the charge recombination on shallow trap surface states. The peak at 416 nm emission is from the de-excitation from lower vibronic levels in the Ti^{4+} 3d states of the TiO_2 lattice to the deep acceptor levels due to surface defects (Marami et al. 2018). The band at 476 nm emission is due to the defect-oriented oxygen vacancies (El Mragui et al. 2019). Since the charge state of the incorporated metal ion and host is not the same, incorporation with the Fe ions causes the generation of oxygen vacancies to maintain the charge neutrality. Due to the defect sites, F-centre formation will be helped and, further, electrons occupying these positions will try to interact with the nearby Ti^{4+} and provide Ti^{3+} ions and F^{+} centres, which is clearly demonstrated for Fe content TiO_2 samples. The PL spectrum at ambient temperature was discerned with various concentrations of Fe in order to determine the behaviour of the photogenerated electron–hole and their recombination rates (Khan et al. 2014). The intensity of peaks decreases with the increase of Fe concentration in the sample which suggests that the electron–hole recombination rate get reduced.

TEM Imaging of Synthesized Nanoparticles

TEM micrographs of synthesized nanoparticles are shown in Fig. 6a. The colour of nanoparticles changes from white to reddish due to iron incorporation in the system can be seen in the Fig. 6c. The 0Fe and 0.1Fe nanoparticle samples are spherical in shape, while high Fe concentration in TiO_2 nanoparticles (0.5Fe and 1Fe) is mainly short rod-shaped. The TEM analysis of the samples showed the transformation from nanospheres to nanorods with

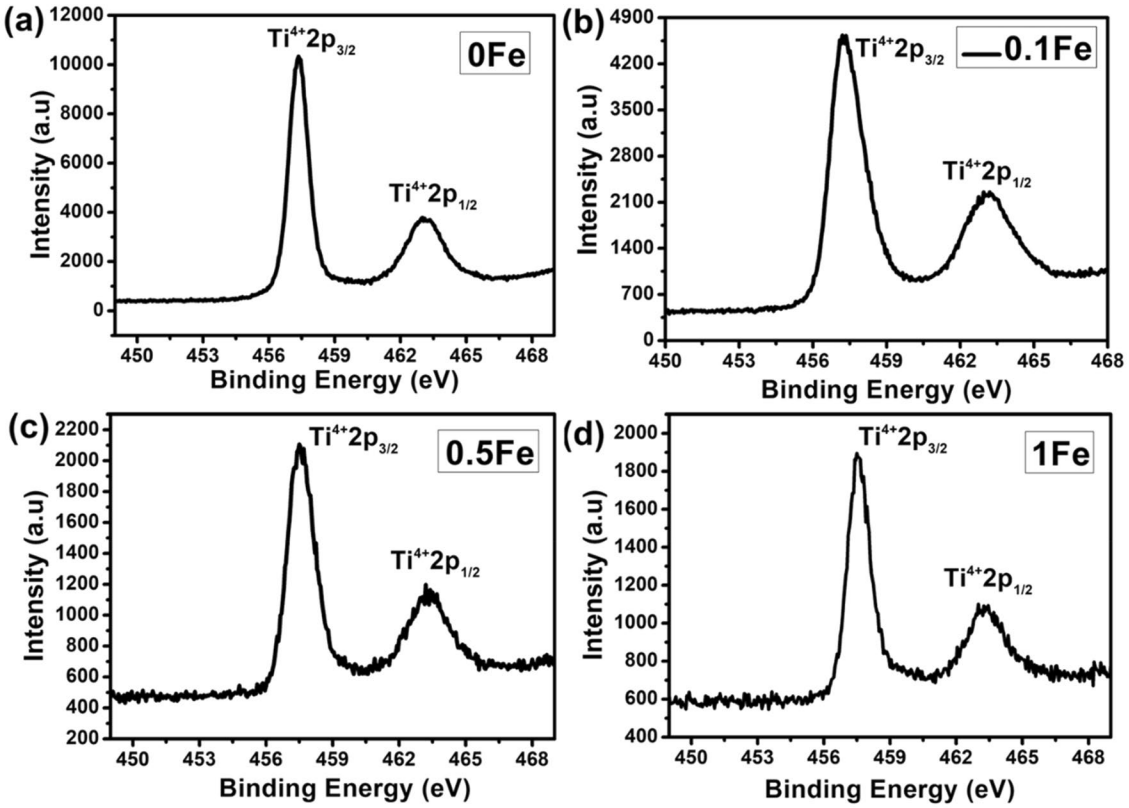

Fig. 4 High-resolution spectra of Ti2p **a** 0Fe, **b** 0.1Fe, **c** 0.5Fe, **d** 1Fe nanoparticles

Table 2 Alteration in ratio of area under the curve for oxygen/Ti ratio after Fe incorporation into TiO_2

Samples	Area		Ratio $Ti2^{4+}p_{3/2}$/O1s	Area		Ratio $Ti2^{4+}p_{1/2}$/Ti_2O_3
	$Ti2^{4+}p_{3/2}$ Peak1	O1s Peak 1		$Ti2^{4+}p_{1/2}$ Peak 2	Ti_2O_3 Peak 2	
0Fe	10,725.29	9910.46	1.08	7841.28	2752.93	2.84
0.1Fe	6871.13	5029.36	1.36	8308.75	5139.04	1.61
0.5Fe	2457.35	2379.99	1.03	2656.45	5775.19	0.45
1Fe	2071.67	2887.53	0.71	2071.67	7715.20	0.26

the incorporation of Fe in TiO_2 crystal. The average size of nanoparticles has been calculated using Image J programme (Vippola et al. 2016). It was estimated that 0Fe and 0.1 Fe have the width of 2.8 nm and 2.7 nm, respectively. The average width for 0.5Fe and 1Fe was calculated as 2.7 nm and 1.5 nm, respectively. The average length for 0.5Fe and 1Fe nanorods was calculated as 26.5 and 25.06 nm, respectively, which is shown in the histogram presenting the size distribution in Fig. 6b. The size got reduced after addition of high concentration of Fe in the TiO_2 matrix. The decrease in diameter and increase in the length of nanorods in 0.5Fe sample were observed. The aspect ratio (length/diameter) of the samples is found to increase from 12 for 0.5Fe and 14 to 1Fe sample with an increase in Fe concentration.

Effect of Synthesized Nanoparticles on Mitochondrial ROS (mtROS) Level

mtROS generating capability of the synthesized TiO_2 and Fe content TiO_2 samples after treating with mitochondrial suspension was studied. A probe DCFH-DA was used to identify the level of oxidative species produced by the synthesized samples at different dosage level. ROS is easily hydrolyzed by esterase in the mitochondrial membrane matrix to the DCFH. Nonfluorescent DCFH is driven to the attacks by ROS which is responsible for the production of fluorescent dichlorofluorescein (DCF) which can be monitored by fluorescence spectrometer. The intensity of fluorescent DCF quantifies the amount of ROS generated in the process (Schanen et al. 2009).

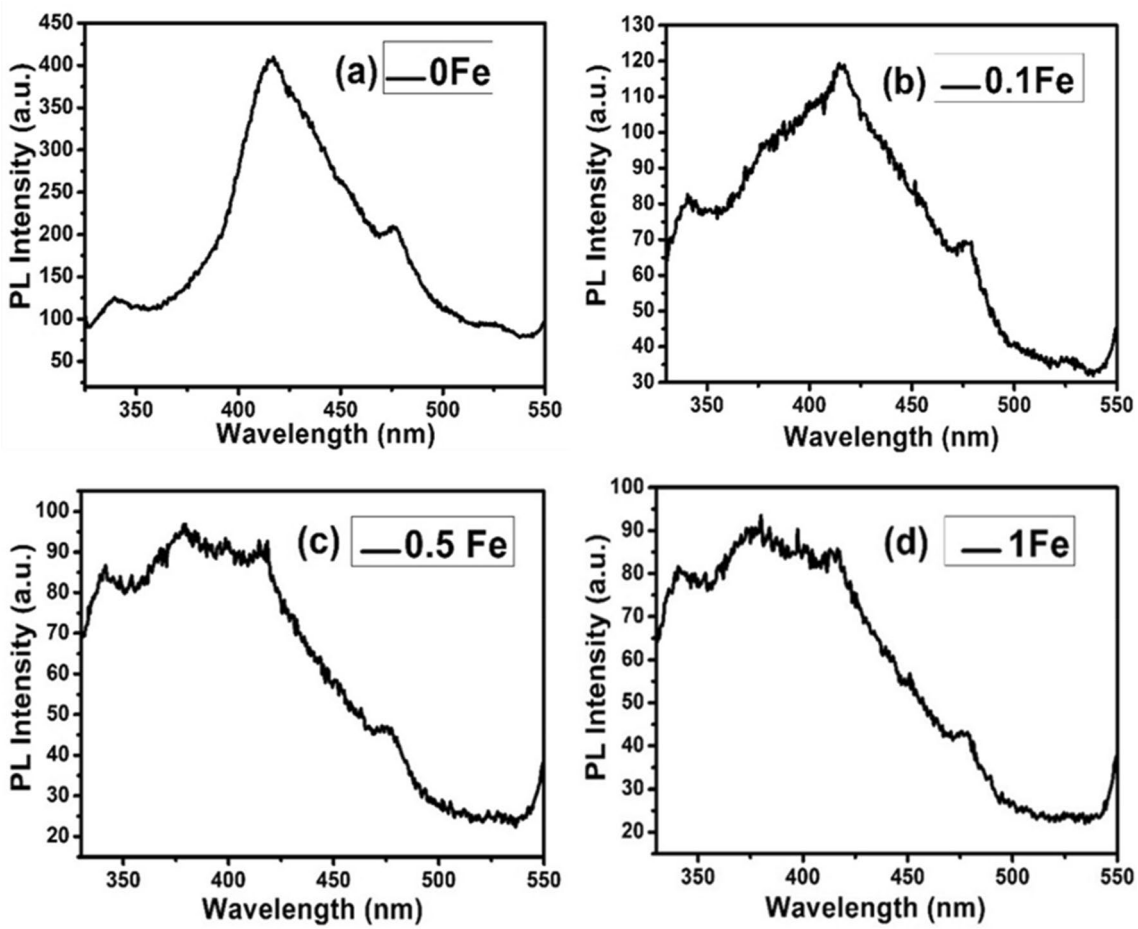

Fig. 5 Photoluminescence spectra of synthesized **a** 0Fe, **b** 0.1Fe, **c** 0.5Fe, and **d** 1Fe nanoparticles

The mtROS generation capacity of 0Fe, 0.1Fe, 0.5Fe, and 1Fe at a varying dosage of 0, 50,100 (µg/mL) is shown in Fig. 7. 0Fe (TiO_2)-treated mitochondrial samples has shown an increase in DCF fluorescence units from a control value of 19.69 up to 25.44 with an increase in dosage. 0.1Fe with 50 µg/mL dose leads to reduce the DCF intensity whereas 100 µg/mL high dose of 0.1Fe containing the maximum titanium ions in comparison to Fe is not able to reduce the superoxide radical anion by trapping them which might be the reason for showing almost similar intensity with control, whereas Fe content TiO_2 samples showed less ROS generation capacity. 0.1Fe, 0.5Fe, and 1Fe-treated mitochondrial samples indicated the decrease in DCF fluorescence units up to 19.81,15.30, and 13.54, respectively, with an increase in Fe concentration and dosage, which means that Fe helps to control the level of ROS generation. The decrease in DCF fluorescence intensity is directly proportional to a decrease in ROS level. Most mtROS are generated as by-products during mitochondrial electron transport. The excessive production of these oxygen-free radicals leads to membrane damage and causes cell death which can be reduced by varying Fe content in TiO_2.

Effect of TiO_2 and Fe Content TiO_2 Nanoparticles on Mitochondria Membrane Potential (MMP)

Nanoparticles exposed to isolated mitochondria could change the membrane potential ($\Delta\psi_m$). In particular, we selected rhodamine 123, a specific probe employed for mitochondria to measure $\Delta\psi_m$. Fluorescent probes have been utilized as optical indicators of the membrane potential alterations in organelles like mitochondria. The technique is based on membrane potential-dependent separation of charged lipophilic dye molecules across the membrane (Baracca et al. 2003). Variations in membrane potential result in changes in the intensity of dye fluorescence or the rate of fluorescence decay. The isolated mitochondria treated with three different dosages (10, 50, 100 µg/mL) of synthesized nanoparticles, i.e. 0Fe, 0.1Fe, 0.5Fe, and 1Fe. The mitochondrial membrane potential was estimated and is depicted in Fig. 8. Reduction in fluorescence units was

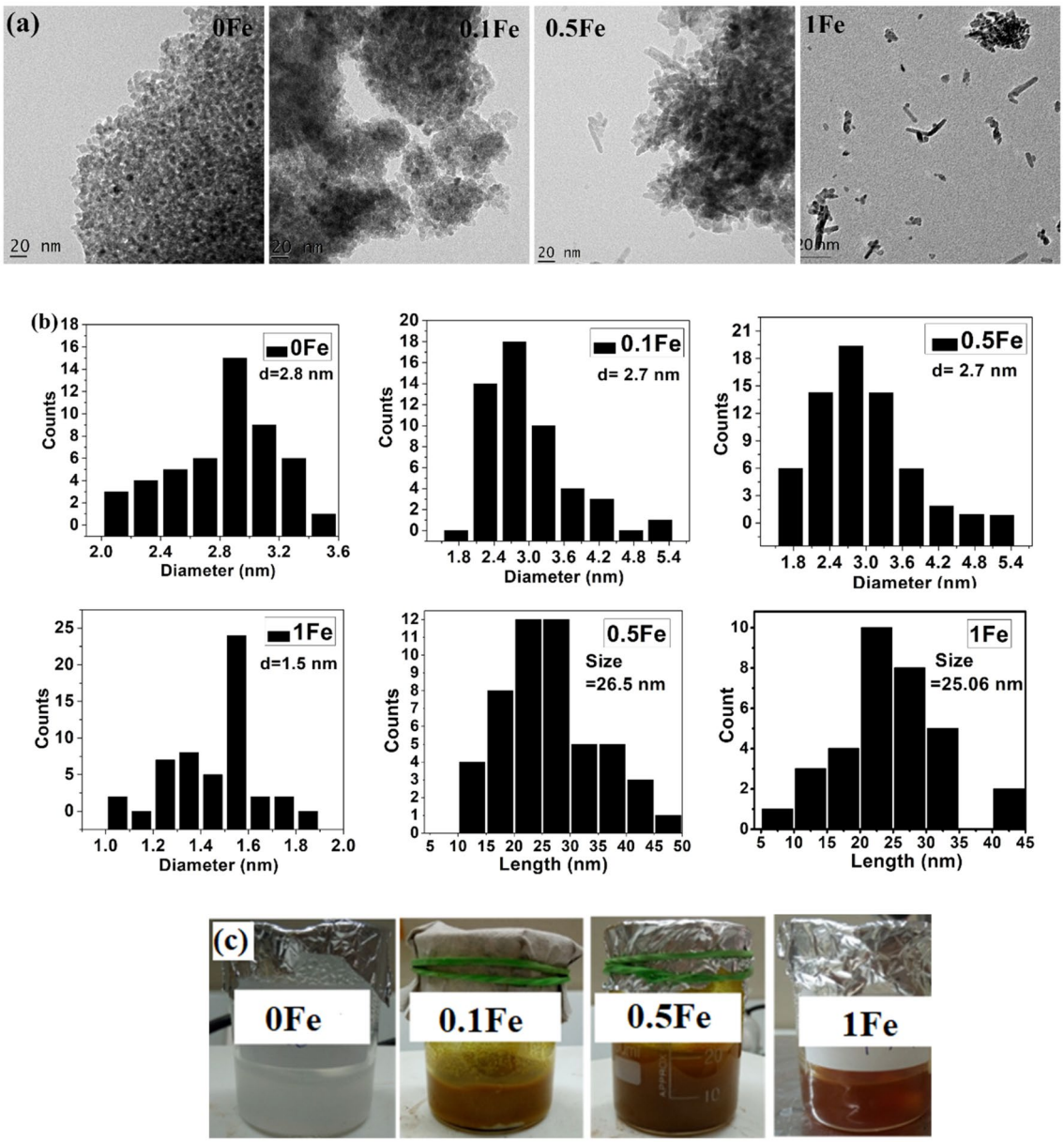

Fig. 6 **a** TEM micrographs of synthesized nanoparticles **b** Size distribution histogram for respective nanoparticles acquired from Image J programme **c** Colour of nanoparticles changes from white to reddish in water

observed after exposure of 0Fe (TiO_2) nanoparticles compared with control, data collected in FL-1 channel which suggested that membrane potential affected by 0Fe. The nonfunctional mitochondria increased with dosage 100 µg/mL of 0Fe sample. Subsequently, the mitochondrial population is not affected by Fe content TiO_2 (0.1Fe, 0.5Fe, 1Fe) nanoparticles treatment; hence, membrane potential was not altered. These results prompted us to further investigate the functional alterations induced by this nanomaterial. 0Fe NPs made the mitochondrial membrane potential of isolated mitochondria decreased from 93.6 to 88.6%. However, treatment with 0.1Fe, 0.5Fe, 1Fe samples stabilized the reduction of mitochondrial membrane potential and maintained it at 95.4%, 96.5%, and 96.9%, respectively, at the dosage of 100 µg/mL. This suggested that Fe incorporation could mitigate TiO_2-induced decline in mitochondrial membrane potential.

Confocal Imaging of Isolated Mitochondria Treated with TiO_2 and Fe Content TiO_2 Nanoparticles

In purpose to determine the mitochondrial membrane collapse, isolated mitochondria were treated with 100 µg/mL dose of each 0Fe, 0.1Fe, 0.5Fe, and 1Fe samples. Rhodamine

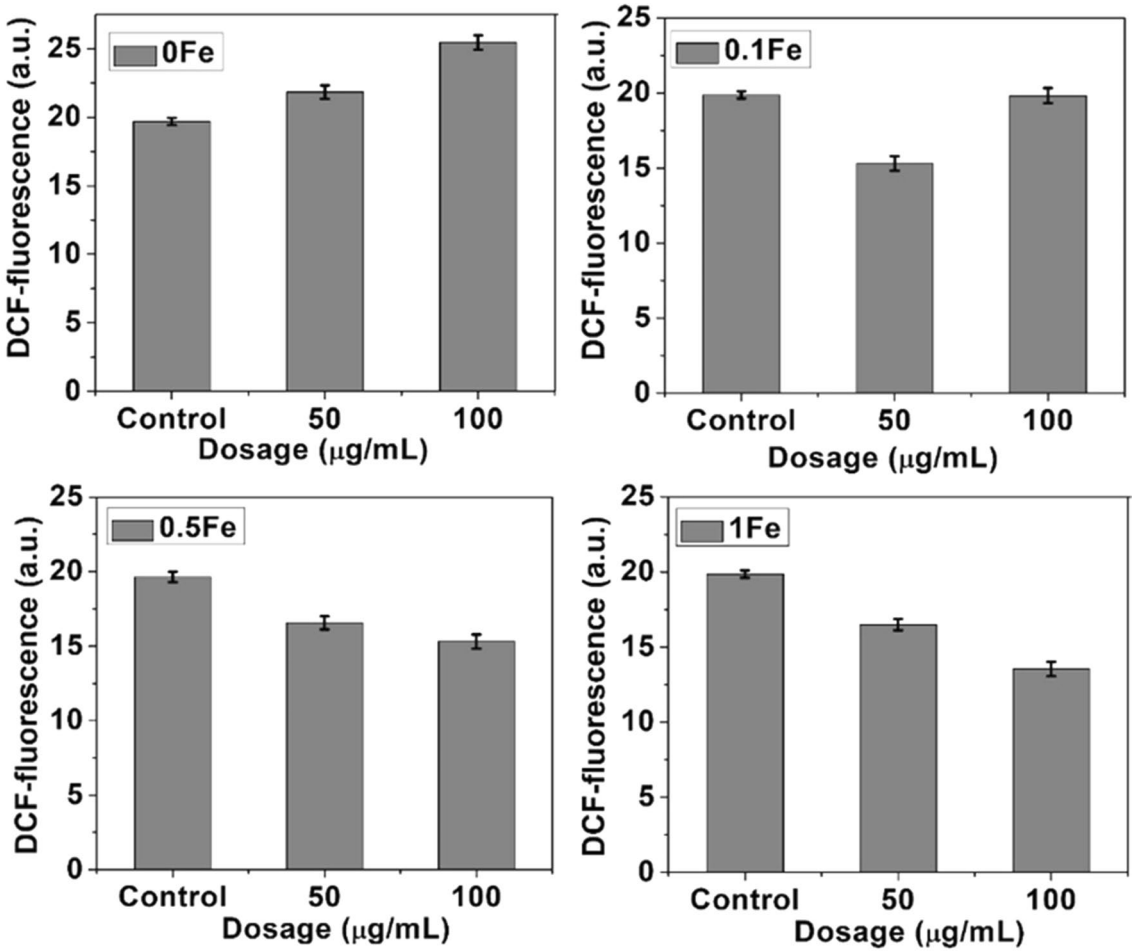

Fig. 7 Dose-dependent ROS production in isolated mitochondria treated with TiO_2 and Fe content TiO_2 nanoparticles

123 was used to image healthy isolated mitochondria which is shown in Fig. 9a. Rhodamine 123 stains mitochondria through binding with mitochondrial protein present on the membrane (Scaduto Jr and Grotyohann 1999). The rhodamine 123 dye creates aggregates with green fluorescence in healthy intact mitochondria. Decrease of mitochondrial membrane potential is indicated by the reduction in green fluorescence treated with 0Fe sample as compared to mitochondria treated with 0.1Fe, 0.5Fe, and 1Fe samples.

Control mitochondrial sample without treated with nanoparticles exhibited green fluorescence due to high $\Delta\psi_m$. Mitochondria treated with 100 μg/mL TiO_2 nanoparticles suspension of 0Fe sample exhibited loss of green aggregate fluorescence representing the depolarization of mitochondrial membrane potential (Natarajan et al. 2015). Depolarization of mitochondrial membrane potential is the initial event which is responsible for mitochondrial dysfunctioning. The stable levels of $\Delta\Psi_m$ and ATP in the cell are kept normal physiological activity due to these factors. However, sustained drop in both factors may be harmful due to nanoparticles exposure which leads to depolarization of mitochondrial membrane potential. Among other factors, $\Delta\Psi_m$ plays a significant role in retaining mitochondrial homeostasis and it is also a driving force for transport of ions (other than H^+) and proteins which are essential for healthy mitochondrial functioning (Vyssokikh et al. 2020). The loss of green mass of green fluorescence observed in the mitochondria treated with 0Fe sample has suggested impairment of membrane, whereas the abundance of green fluorescence was observed in mitochondria treated with Fe content TiO_2 NPs, i.e. 0.1Fe, 0.5Fe, and 1Fe samples, demonstrating the presence of intact and healthy mitochondria. It was observed that, due to the high content of Fe intoTiO_2 matrix, it reduces dissolution of TiO_2 into the medium which prevents depolarization of mitochondrial membrane potential and Fe also assists to maintain the homeostasis at the mitochondrial membrane which ultimately reduces the membrane damage caused through TiO_2 NPs via control of the physiological process at the membrane (Horowitz and Greenamyre 2010). The confocal imaging observation is in

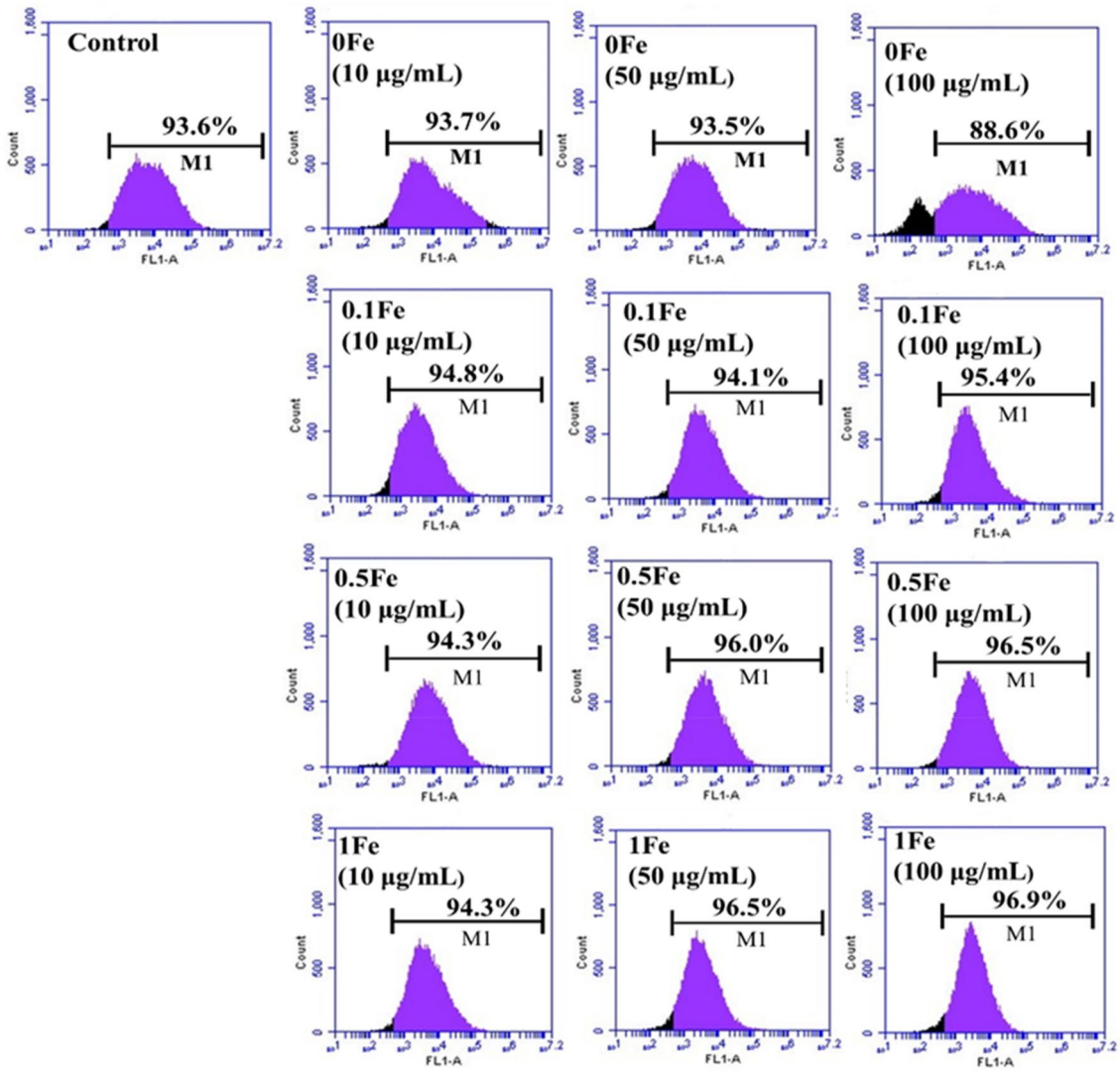

Fig. 8 Dose-dependent representative flow cytometry data showing decline in mitochondria in ratio of functional mitochondria after the exposure of nano-TiO_2 (0Fe) and0.1Fe, 0.5Fe, and 1Fe nanoparticles-treated mitochondria showing the increasing in the membrane potential of mitochondria

consistence with flow cytometry results. Alteration of the proportion of green fluorescence intensity proportion reveals a change in the $\Delta\psi_m$.

Fluorescence intensities were quantified from the marked region in images and presented as a histogram using Image J which is shown in Fig. 9b. The decrease of rhodamine 123 fluorescence has been compared with that of control. The change in arbitrary fluorescence units was incurred to quantify the collapse of mitochondrial membrane potential. The fluorescence unit 58.44 was observed in the control sample, which was later decreased up to 33.71 after treated with 0Fe sample to mitochondria. The fluorescence units of 41.61, 47.76, and 54.63 are observed in 0.1Fe, 0.5Fe, and 1Fe-treated NPs, respectively. The confocal imaging results indicate that with an increase in the incorporation of Fe amount in TiO_2 matrix reduces the toxic effect of TiO_2 on the membrane.

Imaging of Isolated Mitochondrial Membranes Using AFM

For AFM imaging, mica was used as a substrate because of its atomic flat surface that has a minimum effect on the features of mitochondria. AFM offering a means to observe mitochondrial outer membrane protein tubules without the need of fixation or staining process. The surface of the mitochondrial membrane appears quite smooth without wrinkles or particles. The control image of the AFM

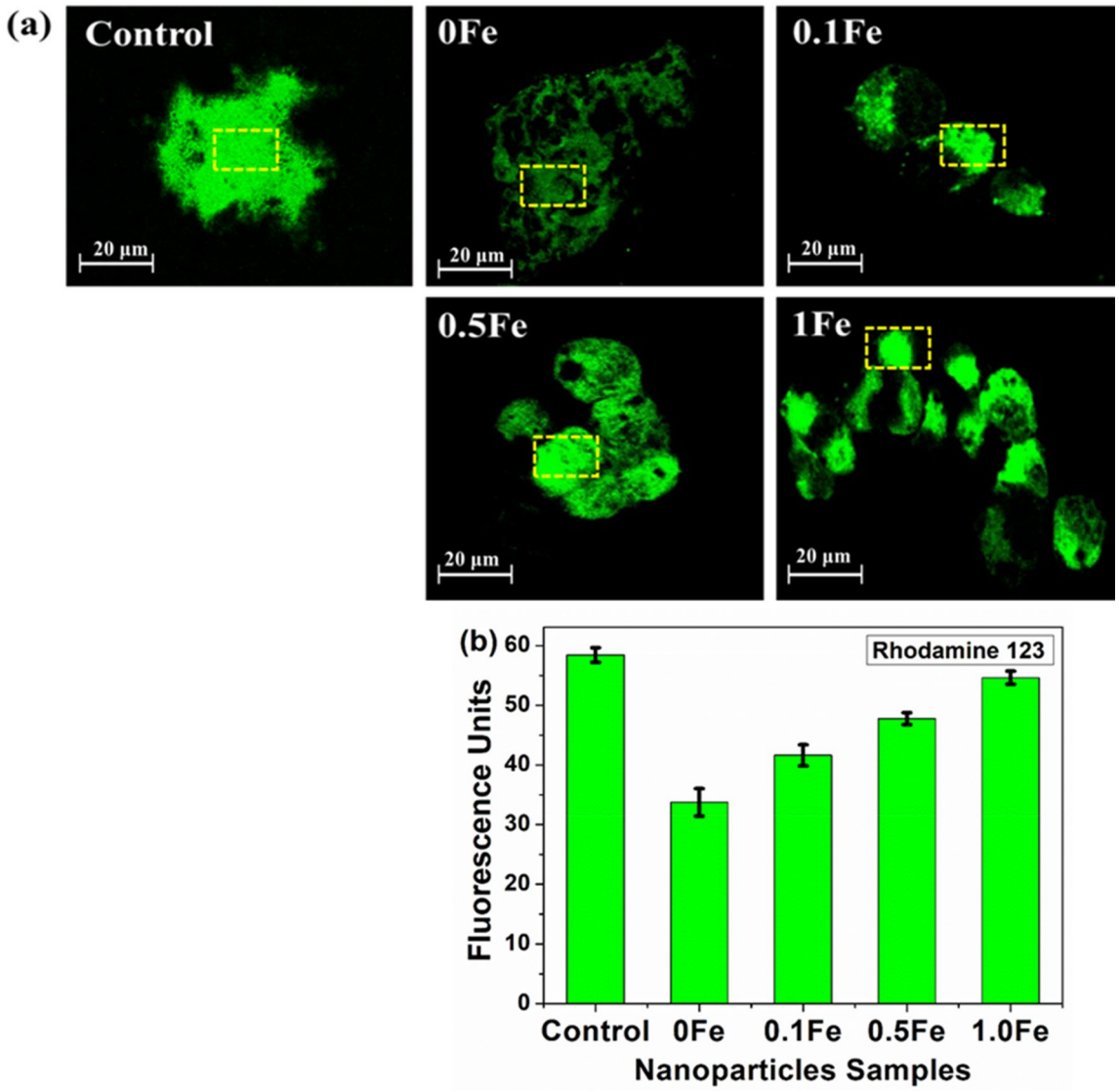

Fig. 9 **a** Confocal microscopic images of nanoparticles treated with isolated mitochondrial suspension and stain with Rhodamine 123 mitochondrial-specific dye **b** Quantification of fluorescence intensity measured from the marked region as shown in confocal images for mitochondrial membrane integrity analysis

showed normal untreated mitochondria in Fig. 10a. Mitochondria under 0Fe (TiO_2) nanoparticles treatment showed fragmented and swelled mitochondrial structures, signifying that the mitochondria were promoted to the fission state by TiO_2 nanoparticles exposure. Then the broken and detached outer membrane was readily adsorbed on the substrate for observation by AFM as shown in Fig. 10b. Moreover, mitochondrial tubule length was considerably shorter in the TiO_2 NPs-treated mitochondrial-rich sample than control mitochondrial sample. It was found that mitochondrial fragmentation in the TiO_2 (100 µg/mL) NPs-treated sample could largely be prevented by Fe incorporation. Fe content TiO_2 (1Fe) sample affect the mitochondrial tubule length neither cause any damage to its morphology. Moreover, Fe supports to reduce the swelling of mitochondria and appear similar to control the image of normal mitochondria which can be seen in Fig. 10c. The swelling and shrinkage difference ratio of mitochondrial tubules from AFM images has been also calculated. In 0Fe (Pure TiO_2) sample, reduction in length from 2 to 1.5 µm and increase in diameter from 0.2 to 0.8 µm were observed. The aspect ratio (length/diameter) of the mitochondria for the control was 10 which get changed to 1.87 in 0Fe sample, whereas no such distortion in length and diameter was observed in 1Fe sample. AFM samples in a buffer solution with exceptional signal-to-noise ratio are presented (García et al. 2007).

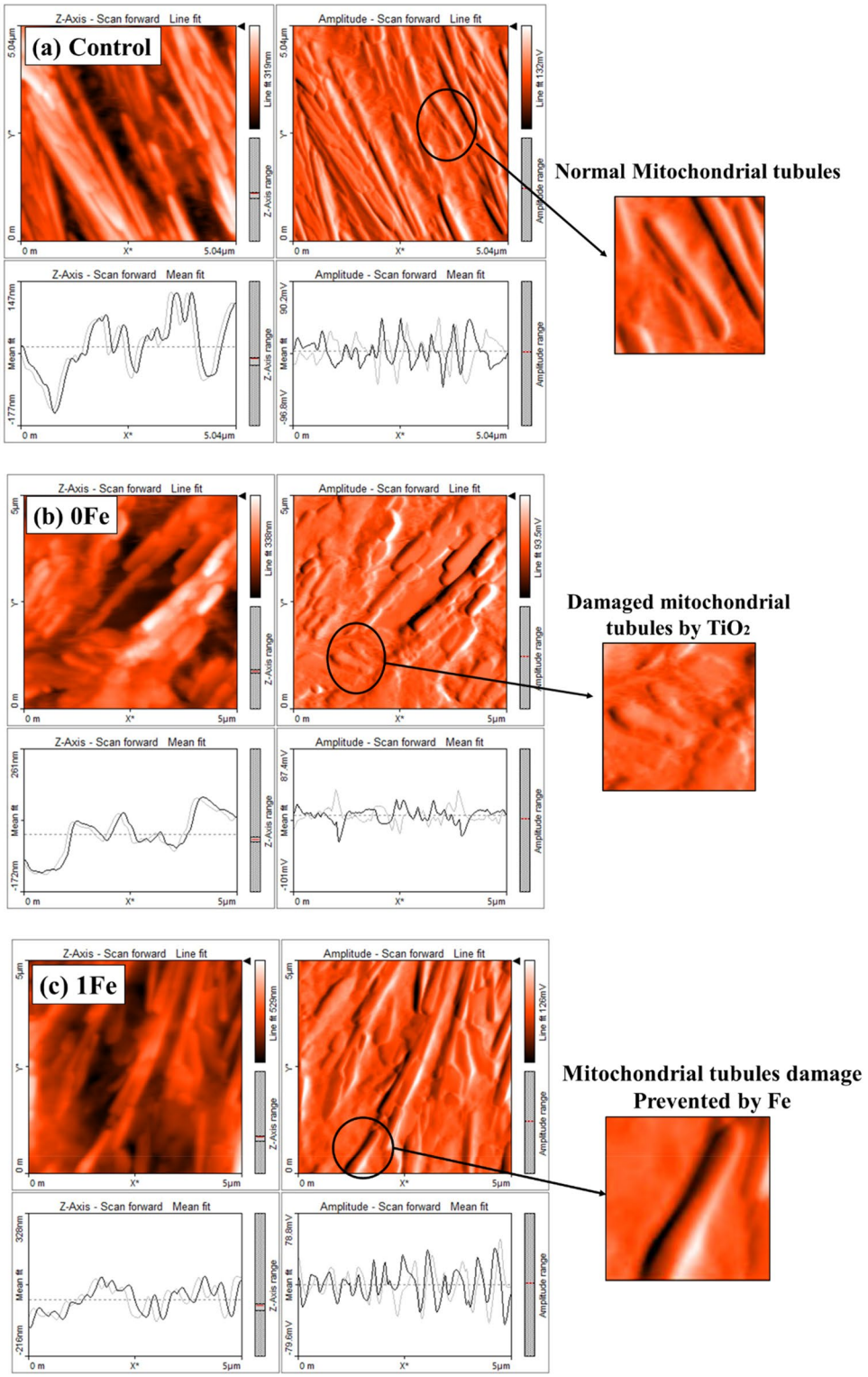

Fig. 10 AFM micrographs of mitochondria in buffer solution **a** control (without nanoparticles treatment) **b** treated with 0Fe, and **c** 1Fe

SERS Analysis of Treated Mitochondrial Protein with Nanoparticles

Surface-enhanced Raman spectroscopy (SERS) has become an essential ultra-sensitive analytical tool for bimolecular analysis of small molecules, proteins, and lipids present on organelle membrane (Bruzas et al. 2018). Specifically, protein and lipid bilayers are dynamic three-dimensional structures that need a label or probe-free methods of characterization. SERS is sensitive enough to sense the formation

of such small nanoparticle aggregates through the enhancement of Raman scattering of biochemical structures in their close surrounding area (Sathuluri et al. 2011). Therefore, the presence of the TiO_2 and Fe content TiO_2 or formation of small aggregates upon interacting with mitochondria was investigated with the SERS technique. SERS survey spectrum of the isolated mitochondria (IM) interacted with synthesized nanoparticles is shown in Fig. 11a. The comparison of all spectra revealed that some of the bands on the spectra obtained from mitochondria were isolated from liver tissue. The bands at around 471, 500–550, 883, 1090, 1460, and 2931 cm^{-1} were observed in isolated mitochondria. The majority of the bands on the mitochondria SERS spectrum can be assigned to protein, lipid, and phospholipids present on inner and outer membranes of mitochondria which can be seen in Table 3 (Brazhe et al. 2015).

The further inspection of the SERS spectrum of mitochondria interacted with 0Fe, 0.5Fe, and 1Fe samples is in contact with bimolecular structures such as protein, lipid, and carbohydrates present on the mitochondria membrane which is shown Fig. 11b. The 0Fe sample shows the absence of the very weak band at 883 cm^{-1} assigned to protein

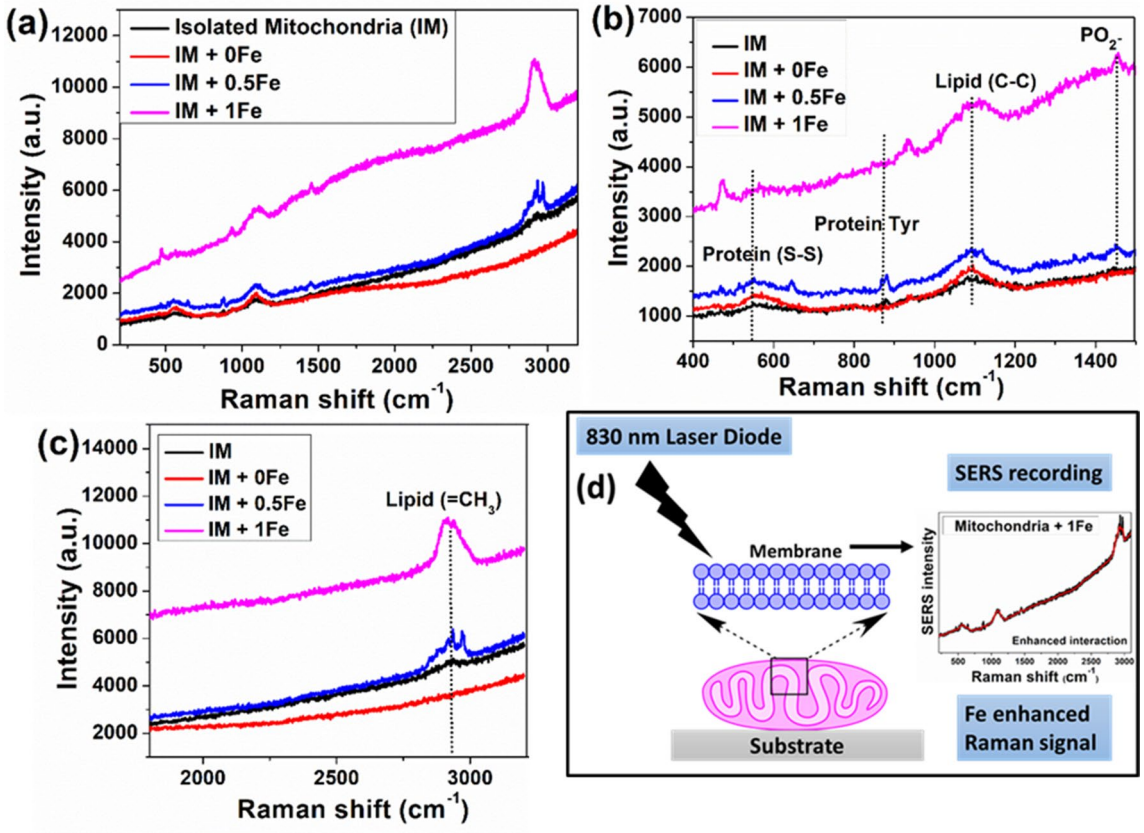

Fig. 11 SERS study of mitochondria treated with nanoparticles **a** survey of Raman spectrum **b** broad view of Raman spectrum from 400 cm^{-1} to 1500 cm^{-1} **c** Raman shift from 2000 to 3000 cm^{-1} **d** scheme of SERS detection which suggested that Fe content TiO_2 nanoparticles interaction enhanced the SERS signal

Table 3 Assignment of the main peaks in SERS spectra of isolated mitochondria

Isolated mitochondria (cm^{-1})	Band assignment	References
471	Glycogen	Rygula et al. (2013) and Bruzas et al. (2018)
500–550	Protein (S–S)	Rygula et al. (2013)
883	Protein (Tyr)	Rygula et al. (2013)
1090	Lipid (P–O)	Czamara et al. (2015) and Bruzas et al. (2018)
1460	Lipid scissor CH_2/CH_3	Czamara et al. (2015)
2931	Lipid (=CH_3)	Czamara et al. (2015)

tyrosine. The weak peak at 2931 cm^{-1} assigned to mitochondrial membrane lipid (=CH_3) disappeared after interaction with (0Fe sample) TiO_2 nanoparticles. A weak intensity of the band at 1090 cm^{-1} originating from PO_2^- group compared to other bands on the spectrum suggests that TiO_2 strongly interacted with this group (Rygula et al. 2013; Czamara et al. 2015), whereas 1Fe sample shows enhancement of the surface interaction due to enhancement of peak intensity of 2931 cm^{-1}. This suggested that Fe content TiO_2 samples have an affinity to bind with lipid structures of the membrane which can be seen in Fig. 11c. Membrane proteins are denatured on the TiO_2 nanoparticle surfaces. Denaturation or loss of activity is suggested to occur through unfavourable interactions between adsorbed proteins. With increase in Fe concentration in the samples, the intensity of all bands was increased in isolated mitochondria treated with 0.5Fe and 1Fe samples without demolition of any bands attributed to mitochondrial proteins and lipids. This acclaimed that Fe content TiO_2 samples enhance the surface activity of mitochondrial membrane without affecting the assigned peaks. The related schematic diagram of SERS detection principle is shown in Fig. 11d which proposed that 1Fe samples give strong and enhanced SERS signal when it binds with lipid and protein structures of the mitochondrial membrane. The results have shown an evident enhancement caused by the Fe incorporation compared to the pure TiO_2. The incorporated Fe ions tend to improve the enrichment of the surface defect state (oxygen vacancies) of TiO_2 and improve the surface properties of the semiconductor TiO_2 NPs and enhance its SERS signal. Surface defects make great contribution to the Fe-TiO_2 charge transfer process. Hence, we employed Fe content TiO_2 NPs as a type of new SERS-active substrate (Ji et al.2019).

Effect of TiO_2 and Fe Content TiO_2 on Mitochondrial Membrane-Associated Proteins

The circular dichroic spectra of mitochondrial membrane-associated proteins were determined. Earlier, negligible nanoparticles–mitochondrial membrane protein interaction analysis has been done using circular dichroism spectroscopy. The secondary structure of the essential membrane proteins and the relative contribution of membrane-associated proteins to the spectrum of the intact membrane were recorded. This secondary structure consists of peptide chain coiled into a right-handed spiral conformation and stabilized by hydrogen bonds between the N–H and the C–O groups in the backbone. It was observed from spectral data of isolated mitochondria, alpha (α)-helical structures protein content were dominated on the membrane (Zahler et al. 1972). This is the major category of transmembrane proteins. The spectrum of mitochondria exhibits minima at 208 and 222 nm characteristic of the α-helical conformation at ellipticity -40° and -47° m degrees, respectively, which is seen in Fig. 12a.

The interaction of pure TiO_2 (0Fe) nanoparticles with mitochondrial membrane protein is shown in Fig. 12b. The spectra evidently demonstrated denaturation of proteins which implicates the disruption and possible demolition of α-helical secondary structures that causes a protein to lose its shape due to oxidative stress triggered by 0Fe interaction which also reduces the ellipticity of the mitochondrial spectrum. While Fe incorporation changes the behaviour of TiO_2 towards the interaction with α-helical structures, therefore denaturation of proteins was prevented due to the Fe which is shown in spectra of Fig. 12c–e. No appreciable change in secondary structure occurs after treating with Fe content TiO_2 nanoparticles which is highlighted with yellow colour in spectra.

Functional Group Assessment of Isolated Mitochondrial Protein

To evaluate the possibility of mitochondrial protein adsorption on the surface of the nanoparticle samples were characterized through FT-IR. Figure 13a shows FT-IR spectra of mitochondrial protein (MP) and nanoparticles loaded with MP (0Fe + MP, 0.1Fe + MP, 0.5Fe + MP, 1Fe + MP). The FT-IR spectrum of MP displays two characteristic bands at 1654.3 cm^{-1} and 1410.4 cm^{-1} named amide I (C=O stretching) and amide II (C–N stretching and N–H bending), respectively. The spectra at 1654.3 cm^{-1} from protein were also attributed to the high proportion of α-helix (Retnakumari et al. 2009). This spectrum determines the relevant region of secondary structure amide I and amide II which is shown in broad view Fig. 13b. The band centred at 3435.8 cm^{-1}can be attributed to primary amines and the band appearing at 1545.6 cm^{-1} can be attributed to strong primary amine scissoring. The broad band appearing at 702.5 cm^{-1} can be attributed to –NH_2 and –NH wagging. The band at 1079.8 cm^{-1} is affiliated to phospholipids, which is a type of lipid molecules present on the membrane of mitochondria (Ahmad et al. 2016).

It was observed from the FT-IR spectrum of nanoparticles loaded with MP grafted in the same spectral region on membrane proteins and lipids. Due to Fe incorporation, shifting was observed in bands of Fe content TiO_2-loaded mitochondrial protein samples. It is difficult to assign absolute those bands to amide I and amide II in nanoparticles-loaded MP samples. Relative intensity changes of overlapped bands were observed in nanoparticles-treated MP. The area under the curve increases in high Fe content TiO_2-loaded MP samples which suggested that bands affiliated to amide II region were showing strong interaction with mitochondrial protein. The band shifting observed at 702.5 cm^{-1} attributed to –NH_2 and –NH wagging after interaction of nanoparticles with MP. The

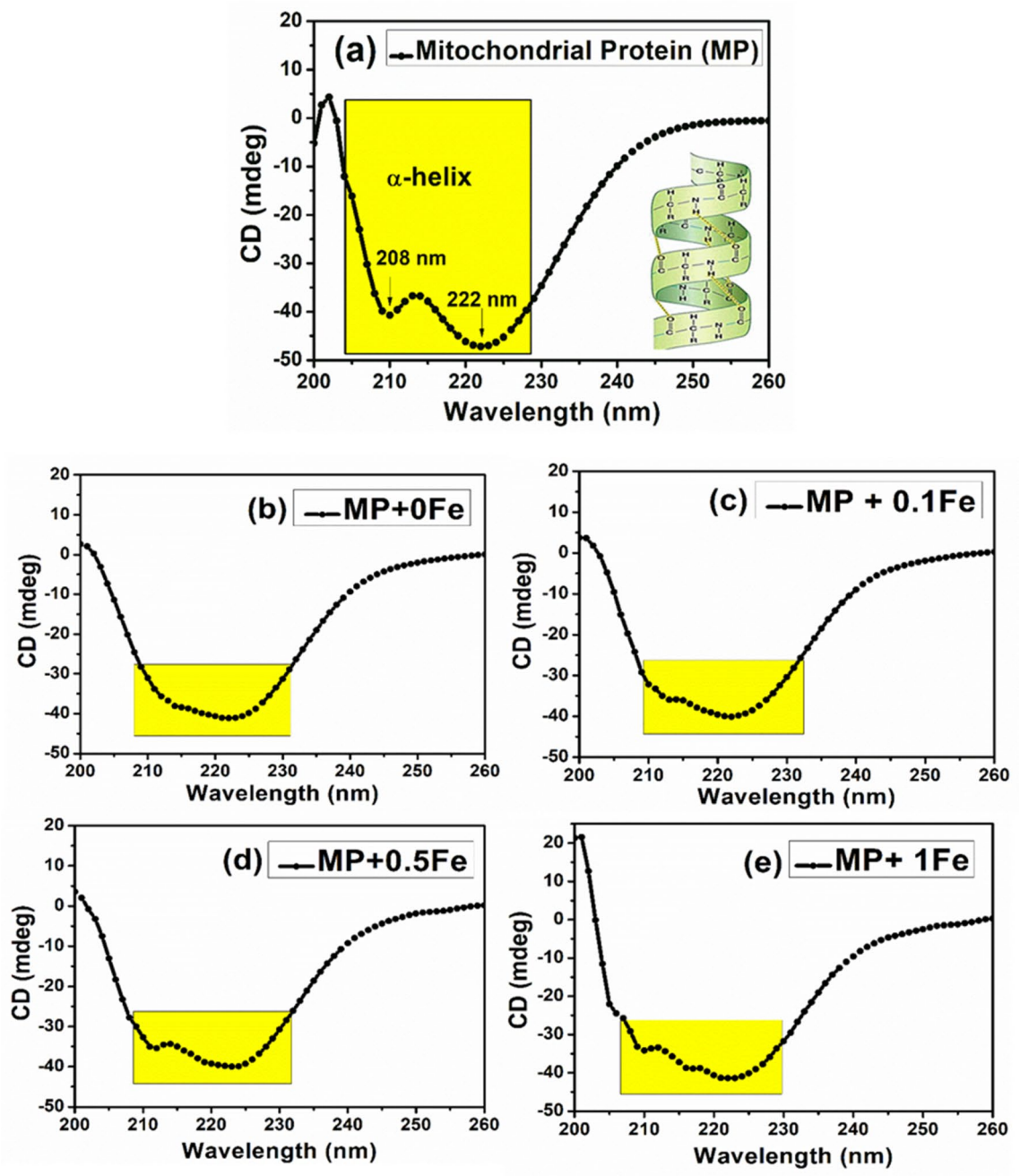

Fig. 12 Circular dichroic spectra of **a** isolated mitochondrial membrane protein and mitochondrial protein treated with **b** 0Fe, **c** 0.1Fe, **d** 0.5Fe, and **e** 1Fe nanoparticles

peak broadening at 3435.8 cm^{-1} has occurred after interaction of Fe content TiO_2 NPs with MP might be due to extensive hydrogen bonding is observed with other hydroxyl groups or changes introduced in the chemical environments.

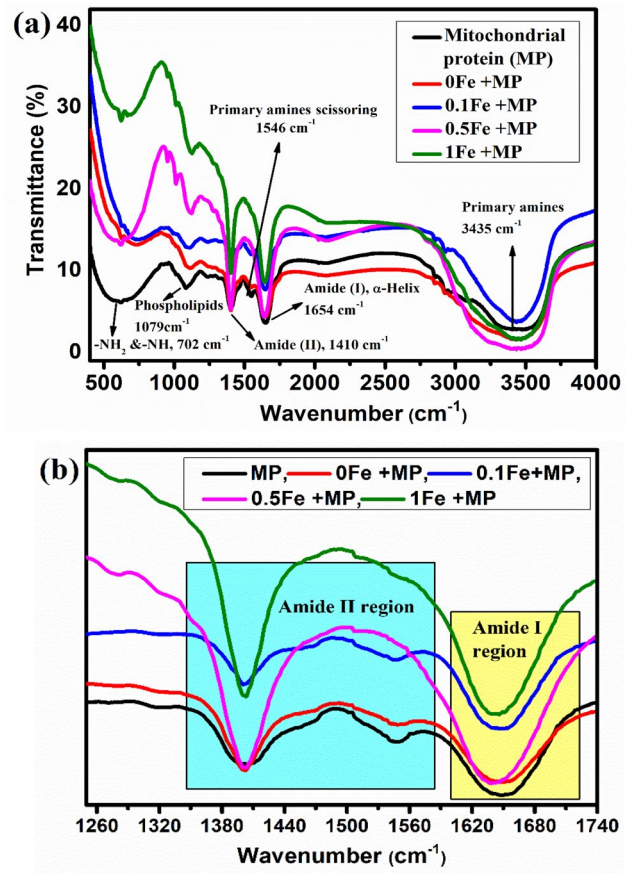

Fig. 13 **a** Survey of FT-IR spectrum of Mitochondrial Protein (MP) interaction with synthesized 0Fe, 0.1Fe, 0.5Fe, and 1Fe nanoparticles **b** broad view FT-IR spectrum of relevant region for determination of protein secondary structure amide I (1600–1700 cm^{-1}) and amide II (1400–1600 cm^{-1})

Toxicity Reduction by Fe^{3+} Incorporated in TiO_2

With summarizing, the key factor of toxic effect is due to the overproduction of ROS on mitochondrial membrane induced by TiO_2 NPs interaction. In the mitochondria, ATP is synthesized by reduction of molecular oxygen to water through a sequence of coupled proton and electron transfer reactions. During this process, as a small percentage of the oxygen remain reduced incompletely because of TiO_2 interaction, which results in the formation of superoxide anion radicals, and subsequently other oxygen-containing radicals which induces toxicity, whereas for Fe-incorporated samples, Fe helps in the reduction process of these oxidative species via maintaining homeostasis across the membrane. Moreover, Fe incorporation transforms the morphology of nano-spherical TiO_2 to nanorod which makes it more biocompatible and less or nontoxic, and therefore, it slows down the rate of dissolution of TiO_2. Later, nanosphere particles can easily enter into membrane compare to nanorod

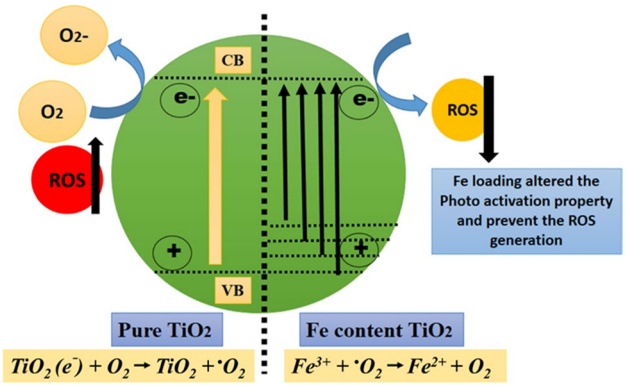

Fig. 14 Mechanism to control the ROS generation via incorporation of Fe^{3+}

through endocytosis process. The SERS analysis proved that Fe incorporated TiO_2 NPs enhances the surface interaction with mitochondrial membrane protein prevents the swelling of mitochondrial tubules and distortion of morphology observed via AFM results. The rhodamine 123 dye aggregates with protein present on the functional and intact mitochondrial membrane which ultimately increases the intensity of green fluorescence investigated through confocal imaging and flow cytometry.

Mechanism Behind Toxicity Reduction by Fe

The fast dissolution of TiO_2 NPs and the role of dissolved titanium ions is a major factor responsible for toxicity. It has been shown that Fe ion improves the structural and thermodynamic stability of TiO_2 NPs. Purposeful reduction of TiO_2 toxicity was attained by iron incorporation, which changed the material matrix to slow Ti^{4+} release. Moreover, structural and morphological modification of TiO_2 is done by Fe addition. This also controls the overproduction of mitochondrial reactive oxygen species by Fe^{3+} and helps in reduction of toxicity. Figure 14 explains the mechanism of toxicity prevention of TiO_2 via incorporation of Fe^{3+}. This figure shows that semiconducting nano-TiO_2 induces the production of ROS such as superoxide anions (O_2^-) because of its photo-activation property. Fe^{3+} incorporation alters the photo-activation property, hence controls the ROS generation by TiO_2 (Barkhade et al. 2021).

Conclusion

The sol–gel synthesis method proved to be low cost and does not need any sophisticated instruments for preparing the 0Fe, 0.1Fe, 0.5Fe, and 1Fe nanoparticle samples with controlled size and morphology. The XRD and TEM micrograph suggested the successful phase and structural transformation of

the synthesized anatase TiO_2 nanosphere into rutile nanorods with the existence of iron oxide at 400 °C. XPS spectrum also revealed that $Ti^{4+}$is present in pure TiO_2 and Fe^{3+}ionic state is present in samples with a minor portion of Fe^{2+} ions in Fe content TiO_2 nanoparticles. The toxicological study of synthesized nanoparticles TiO_2 and Fe content TiO_2 towards isolated mitochondria was undertaken using AFM, SERS, flow cytometry, and confocal imaging. The results of AFM suggested that nano-TiO_2 enters into the mitochondrial membrane and interacted with membrane protein tubules and leads to the destruction of mitochondrial morphology. CD spectrum also shows that TiO_2 denatures the α-helical structure membrane protein which can be co-related with FT-IR study. The fluorescence units decrease from 58.44 to 33.71 because of no agglomeration of Rh123 dye on the membrane was observed after TiO_2 interaction. SERS results suggested that Fe content TiO_2 enhanced surface interaction with phospholipids, protein, and carbohydrates. At dosage of 100 μg/mL, TiO_2 leads to an increase in the numbers of nonfunctional mitochondria which was detected by flow cytometry after a decline in membrane potential. In conclusion, the toxicological effect of TiO_2 was prevented by Fe incorporation and Fe leads to an increase in the membrane potential of mitochondria via a nonspecific approach.

Acknowledgements The first author is grateful to the Indian Government (UGC) for the award of scholarship. The authors wish to thank Central Instrumentation Facility, Central University of Punjab, India, for Flow Cytometry and Confocal Microscopy facilities. Thanks are also extended to Department of Physics, Savitribai Phule Pune University and IR &D, Gujarat Forensic Science University, India, for other characterization facilities.

Data Availability The datasets generated during and/or analysed during the current study are available from the corresponding author on reasonable request.

Compliance with Ethical Standards

Conflict of interest There are no conflicts of interest to declare.

References

Abidov A, Allabergenov B, Lee J, Jeon HW, Jeong SW, Kim S (2013) X-ray photoelectron spectroscopy characterization of Fe doped TiO_2 photocatalyst. Int J Mater Mech Manuf 1:294–296

Ahmad F, Zhou Y, Ling Z, Xiang Q, Zhou X (2016) Systematic elucidation of interactive unfolding and corona formation of bovine serum albumin with cobalt ferrite nanoparticles. RSC Adv 6:35719–35730

Akshay VR, Arun B, Mandal G, Chanda A, Vasundhara M (2019) Significant reduction in the optical band-gap and defect assisted magnetic response in Fe-doped anatase TiO_2 nanocrystals as dilute magnetic semiconductors. New J Chem 43:6048–6062

Ali T, Tripathi P, Azam A, Raza W, Ahmed AS, Ahmed A, Muneer M (2017) Photocatalytic performance of Fe-doped TiO_2 nanoparticles under visible-light irradiation. Mater Res Express 4:1–12

Banerjee K, Thiagarajan P (2014) A review of titanium Di oxide nanoparticles-synthesis, applications and toxicity concerns. Nanosci Nanotechnol-Asia 4:132–143

Bapna K, Phase DM, Choudhary RJ (2011) Study of valence band structure of Fe doped anatase TiO_2 thin films. J Appl Phys 110:1–6

Baracca A, Sgarbi G, Solaini G, Lenaz G (2003) Rhodamine 123 as a probe of mitochondrial membrane potential: evaluation of proton flux through F0 during ATP synthesis. Biochim Biophys Acta (BBA) 1606:137–146

Barkhade T, Mishra S, Chander H, Mahapatra SK, Banerjee I (2019c) Effect of TiO_2 and Fe doped TiO_2 nanoparticles on mitochondrial membrane potential in HBL-100 cells. Biointerphases 14:1–10

Barkhade T, Phatangare A, Dahiwale S, Mahapatra SK, Banerjee I (2019b) Nano-bio interface study between Fe content TiO_2 nanoparticles and adenosine triphosphate biomolecules. Surf Interface Anal 51:894–905

Barkhade T, Mahapatra SK, Banerjee I (2019a) Study of mitochondrial swelling, membrane fluidity and ROS production induced by nano-TiO_2 and prevented by Fe incorporation. Toxicol Res 8:711–722

Barkhade T, Indoliya A, Poddar R, Mahapatra SK, Banerjee I (2021) Iron content titanium dioxide nanoparticles as exogenous contrast agent for tissue imaging using swept-source optical coherence tomography. AIP Adv 11(1):015023

Bennat C, Müller-Goymann CC (2000) Skin penetration and stabilization of formulations containing microfine titanium dioxide as physical UV filter. Int J Cosmet Sci 22:271–283

Bharti B, Kumar S, Lee HN, Kumar R (2016) Formation of oxygen vacancies and Ti^{3+} state in TiO_2 thin film and enhanced optical properties by air plasma treatment. Sci Rep 6:1–12

Brazhe NA, Evlyukhin AB, Goodilin EA, Semenova AA, Novikov SM, Bozhevolnyi SI, Chichkov BN, Sarycheva AS, Baizhumanov AA, Nikelshparg EI, Deev LI (2015) Probing cytochrome c in living mitochondria with surface-enhanced Raman spectroscopy. Sci Rep 5:1–13

Bruzas I, Lum W, Gorunmez Z, Sagle L (2018) Advances in surface-enhanced Raman spectroscopy (SERS) substrates for lipid and protein characterization: sensing and beyond. Analyst 143(17):3990–4008

Chen J, Dong X, Zhao J, Tang G (2009) In vivo acute toxicity of titanium dioxide nanoparticles to mice after intraperitioneal injection. J Appl Toxicol 29:330–337

Chen Q, Wang N, Zhu M, Lu J, Zhong H, Xue X, Guo S, Li M, Wei X, Tao Y, Yin H (2018) TiO_2 nanoparticles cause mitochondrial dysfunction, activate inflammatory responses, and attenuate phagocytosis in macrophages: a proteomic and metabolomic insight. Redox Biol 15:266–276

Chibber S, Agarwal K (2017) Titanium dioxide (TiO_2) nanoparticles induced ROS generation and its effect on cellular antioxidant defense in WRL ndash cell. MOJ Bioequiv Bioavail 3:70–74

Czamara K, Majzner K, Pacia MZ, Kochan K, Kaczor A, Baranska M (2015) Raman spectroscopy of lipids: a review. J Raman Spectrosc 46(1):4–20

Donaldson K, Stone V, Gilmour PS, Brown DM, MacNee W (2000) Ultrafine particles: mechanisms of lung injury. Philos Trans R Soc Lond 358:2741–2749

El Mragui A, Logvina Y, Pinto da Silva L, Zegaoui O, Esteves da Silva JC (2019) Synthesis of Fe-and Co-doped TiO_2 with improved photocatalytic activity under visible irradiation toward carbamazepine degradation. Materials 12(23):3874

Elsaesser A, Howard CV (2012) Toxicology of nanoparticles. Adv Drug Deliv Rev 64:129–137

Flak D, Coy E, Nowaczyk G, Yate L, Jurga S (2015) Tuning the photodynamic efficiency of TiO_2 nanotubes against HeLa cancer cells by Fe-doping. RSC Adv 5:85139–85152

Freyre-Fonseca V, Delgado-Buenrostro NL, Gutiérrez-Cirlos EB, Calderón-Torres CM, Cabellos-Avelar T, Sánchez-Pérez Y, Pinzón E, Torres I, Molina-Jijón E, Zazueta C, Pedraza-Chaverri J (2011) Titanium dioxide nanoparticles impair lung mitochondrial function. Toxicol Lett 202:111–119

García R, Magerle R, Perez R (2007) Nanoscale compositional mapping with gentle forces. Nat Mater 6:405–411

George S, Pokhrel S, Ji Z, Henderson BL, Xia T, Li L, Zink JI, Nel AE, Mädler L (2011) Role of Fe doping in tuning the band gap of TiO_2 for the photo-oxidation-induced cytotoxicity paradigm. J Am Chem Soc 133:11270–11278

Hirano M, Joji T, Inagaki M, Iwata H (2004) Direct formation of iron (III)-doped titanium oxide (anatase) by thermal hydrolysis and its structural property. J Am Ceram Soc 87:35–41

Horowitz MP, Greenamyre JT (2010) Mitochondrial iron metabolism and its role in neurodegeneration. J Alzheimer's Dis 20:S551–S568

Hwang JS, Yu J, Kim HM, Oh JM, Choi SJ (2019) Food additive titanium dioxide and its fate in commercial foods. Nanomaterials 9:1175

Jacobs JF, Van de Poel I, Osseweijer P (2010) Sunscreens with titanium dioxide (TiO_2) nano-particles: a societal experiment. NanoEthics 4:103–113

Jefferson DA (2000) The surface activity of ultrafine particles. In: Brown LM, Collings N, Harrison RM, Maynard RL, Maynard AD (eds) Ultrafine particles in the atmosphere. World Scientific, Singapore, pp 155–167

Ji P, Mao Z, Wang Z, Xue X, Zhang Y, Lv J, Shi X (2019) Improved surface-enhanced Raman scattering properties of ZrO_2 nanoparticles by Zn doping. Nanomaterials 9(7):983

Jin CY, Zhu BS, Wang XF, Lu QH (2008) Cytotoxicity of titanium dioxide nanoparticles in mouse fibroblast cells. Chem Res Toxicol 21(9):871–1877

Kelly SM, Price NC (2000) The use of circular dichroism in the investigation of protein structure and function. Curr Protein Pept Sci 1:349–384

Khan W, Ahmad S, Hassan MM, Naqvi AH (2014) Structural phase analysis, band gap tuning and fluorescence properties of Co doped TiO_2 nanoparticles. Opt Mater 38:278–285

Kreyling WG, Semmler M, Erbe F, Mayer P, Takenaka S, Schulz H, Oberdörster G, Ziesenis A (2002) Translocation of ultrafine insoluble iridium particles from lung epithelium to extrapulmonary organs is size dependent but very low. J Toxicol Environ Health 65:1513–1530

Leedahl B, Zatsepin DA, Boukhvalov DW, Green RJ, McLeod JA, Kim SS, Kurmaev EZ, Zhidkov IS, Gavrilov NV, Cholakh SO, Moewes A (2014) Structural defects induced by Fe-ion implantation in TiO_2. J Appl Phys 115:1–8

Li M, Pokhrel S, Jin X, Mädler L, Damoiseaux R, Hoek EM (2011) Stability, bioavailability, and bacterial toxicity of ZnO and iron-doped ZnO nanoparticles in aquatic media. Environ Sci Technol 45:755–761

Marami MB, Farahmandjou M, Khoshnevisan B (2018) Sol–gel synthesis of Fe-doped TiO_2 nanocrystals. J Electron Mater 47(7):3741–3748

Mathews NR, Jacome MC, Angeles-Chavez C, Antonio JT (2015) Fe doped TiO_2 powder synthesized by sol gel method: structural and photocatalytic characterization. J Mater Sci 26:5574–5584

Mavon A, Miquel C, Lejeune O, Payre B, Moretto P (2007) In vitro percutaneous absorption and in vivo stratum corneum distribution of an organic and a mineral sunscreen. Skin Pharmacol Physiol 20:10–20

Nasralla N, Yeganeh M, Astuti Y, Piticharoenphun S, Shahtahmasebi N, Kompany A, Karimipour M, Mendis BG, Poolton NRJ, Šiller L (2013) Structural and spectroscopic study of Fe-doped TiO_2 nanoparticles prepared by sol–gel method. Scientia Iranica 20:1018–1022

Natarajan V, Wilson CL, Hayward SL, Kidambi S (2015) Titanium dioxide nanoparticles trigger loss of function and perturbation of mitochondrial dynamics in primary hepatocytes. PLoS ONE 10:1–19

Oberdörster G, Oberdörster E, Oberdörster J (2005) Nanotoxicology: an emerging discipline evolving from studies of ultrafine particles. Environ Health Perspect 113:823–839

Osmond-McLeod MJ, Oytam Y, Osmond RI, Sobhanmanesh F, McCall MJ (2014) Surface coatings protect against the in vitro toxicity of zinc oxide nanoparticles in human hepatic stellate cells. J Nanomed Nanotechnol 5:1–8

Pelaz B, del Pino P, Maffre P, Hartmann R, Gallego M, Rivera-Fernandez S, de la Fuente JM, Nienhaus GU, Parak WJ (2015) Surface functionalization of nanoparticles with polyethylene glycol: effects on protein adsorption and cellular uptake. ACS Nano 9:6996–7008

Retnakumari A, Setua S, Menon D, Ravindran P, Muhammed H, Pradeep T, Nair S, Koyakutty M (2009) Molecular-receptor-specific, non-toxic, near-infrared-emitting Au cluster-protein nanoconjugates for targeted cancer imaging. Nanotechnology 21:1–12

Rygula A, Majzner K, Marzec KM, Kaczor A, Pilarczyk M, Baranska M (2013) Raman spectroscopy of proteins: a review. J Raman Spectrosc 44(8):1061–1076

Saleh NB, Milliron DJ, Aich N, Katz LE, Liljestrand HM, Kirisits MJ (2016) Importance of doping, dopant distribution, and defects on electronic band structure alteration of metal oxide nanoparticles: implications for reactive oxygen species. Sci Total Environ 568:926–932

Santonastaso M, Mottola F, Colacurci N, Iovine C, Pacifico S, Cammarota M, Cesaroni F, Rocco L (2019) In vitro genotoxic effects of titanium dioxide nanoparticles (n-TiO_2) in human sperm cells. Mol Reprod Dev 86:1369–1377

Sathuluri RR, Yoshikawa H, Shimizu E, Saito M, Tamiya E (2011) Gold nanoparticle-based surface-enhanced Raman scattering for noninvasive molecular probing of embryonic stem cell differentiation. PLoS ONE 6:1–13

Scaduto RC Jr, Grotyohann LW (1999) Measurement of mitochondrial membrane potential using fluorescent rhodamine derivatives. Biophys J 76:469–477

Schanen BC, Karakoti AS, Seal S, Drake DR III, Warren WL, Self WT (2009) Exposure to titanium dioxide nanomaterials provokes inflammation of an in vitro human immune construct. ACS Nano 3:2523–2532

Takenaka S, Karg E, Roth C, Schulz H, Ziesenis A, Heinzmann U, Schramel P, Heyder J (2001) Pulmonary and systemic distribution of inhaled ultrafine silver particles in rats. Environ Health Perspect 109:547–551

Trouiller B, Reliene R, Westbrook A, Solaimani P, Schiestl RH (2009) Titanium dioxide nanoparticles induce DNA damage and genetic instability in vivo in mice. Cancer Res 69:8784–8789

Vippola M, Valkonen M, Sarlin E, Honkanen M, Huttunen H (2016) Insight to nanoparticle size analysis-novel and convenient image analysis method versus conventional techniques. Nanoscale Res Lett 11:1–9

Vyssokikh MY, Holtze S, Averina OA, Lyamzaev KG, Panteleeva AA, Marey MV, Skulachev VP (2020) Mild depolarization of the inner mitochondrial membrane is a crucial component of an anti-aging program. Proc Natl Acad Sci 117(12):6491–6501

Wang J, Zhou G, Chen C, Yu H, Wang T, Ma Y, Jia G, Gao Y, Li B, Sun J, Li Y (2007) Acute toxicity and biodistribution of different sized titanium dioxide particles in mice after oral administration. Toxicol Lett 168:176–185

Wang E, Yang W, Cao Y (2009) Unique surface chemical species on indium doped TiO_2 and their effect on the visible light photocatalytic activity. J Phys Chem C 113:20912–20917

Warheit DB, Webb TR, Reed KL, Frerichs S, Sayes CM (2007) Pulmonary toxicity study in rats with three forms of ultrafine-TiO_2 particles: differential responses related to surface properties. Toxicology 230:90–104

Weir A, Westerhoff P, Fabricius L, Hristovski K, Von Goetz N (2012) Titanium dioxide nanoparticles in food and personal care products. Environ Sci Technol 46:2242–2250

Wu J, Liu W, Xue C, Zhou S, Lan F, Bi L, Xu H, Yang X, Zeng FD (2009) Toxicity and penetration of TiO_2 nanoparticles in hairless mice and porcine skin after subchronic dermal exposure. Toxicol Lett 191:1–8

Xia T, Zhao Y, Sager T, George S, Pokhrel S, Li N, Schoenfeld D, Meng H, Lin S, Wang X, Wang M (2011) Decreased dissolution of ZnO by iron doping yields nanoparticles with reduced toxicity in the rodent lung and zebrafish embryos. ACS Nano 5:1223–1235

Yang LY, Gao JL, Gao T, Dong P, Ma L, Jiang FL, Liu Y (2016) Toxicity of polyhydroxylated fullerene to mitochondria. J Hazard Mater 301:119–126

Zahler WL, Puett D, Fleischer S (1972) Circular dichroism of mitochondrial membranes before and after extraction of lipids and surface proteins. Biochim Biophys Acta (BBA) 255(1):365–379

Authors and Affiliations

Tejal Barkhade[1] · Santosh Kumar Mahapatra[2] · Indrani Banerjee[1]

[1] School of Nanosciences, Central University of Gujarat, Gandhinagar, Gujarat 382030, India

[2] Department of Physical Science, Central University of Punjab, Bathinda 151001, Punjab, India